

1 **Actin networks modulate heterogenous NF- κ B dynamics in response to**

2 **TNF α**

3 Francesca Butera^{1,3,*}, Julia E. Sero², Lucas G. Dent¹, Chris Bakal¹

4 ¹Chester Beatty Laboratories, Division of Cancer Biology, Institute of Cancer
5 Research, 237 Fulham Road, London, SW3 6JB, UK

6 ²Biology and Biochemistry Department, Bath University, Claverton Down, BA2 7AY,
7 UK

8 ³Lead contact

9 *Correspondence: francesca.butera@icr.ac.uk

10

11

12

13

14

15

16

17

18

19 **Abstract**

20 The canonical NF- κ B transcription factor RELA is a master regulator of immune
21 and stress responses and is commonly upregulated in PDAC tumours. Using live
22 imaging, we characterised single cell RELA translocation dynamics in two human
23 PDAC cell lines and identified high cell-to-cell variability in RELA responses to
24 TNF α , including unresponsive, damped, and sustained nuclear RELA localisation.
25 Using a combination of quantitative single cell imaging and Bayesian analysis, we
26 determined that heterogeneity in RELA nuclear translocation between and within
27 PDAC cell lines is dependent on cytoskeletal organisation, in particular actin
28 abundance and distribution. Subsequently, RELA nuclear localisation could be up
29 or downregulated through biochemical modulation of cell shape and the
30 cytoskeleton, particularly by disrupting nucleation of actin stress fibres and
31 branched actin via formin and ARP2/3 inhibition. Together, our data provide
32 evidence that actin configuration regulates RELA translocation during the
33 inflammatory response and that targeting actin dynamics can be used to modulate
34 misregulated NF- κ B signalling in PDAC.

35

36

37

38

39

40

41

42 **Introduction**

43 The NF- κ B transcription factor RELA is an essential mediator of the inflammatory
44 and immune responses in all mammals (Hayden et al., 2006) and is central to the
45 canonical NF- κ B signalling pathway (Ghosh et al., 1998). As a transcription factor,
46 RELA activation is controlled in large part through its subcellular localisation.
47 Inactive RELA is sequestered in the cytoplasm by I κ B proteins. Degradation of I κ B
48 by upstream cues, such as the potent inflammatory cytokine Tumour Necrosis
49 Factor α (TNF α), enables RELA translocation to the nucleus where it regulates
50 gene expression (DiDonato et al., 1997; Zandi et al., 1997).

51 Live imaging experiments using RELA localisation and activity reporters have
52 shown that RELA oscillates between the nucleus and cytoplasm in response to
53 TNF α (Nelson et al., 2004; Tay et al., 2010; Sero et al., 2015; Zambrano et al.,
54 2016). Oscillations are driven by a negative feedback loop between RELA and
55 particular I κ B family members, since the genes encoding I κ B proteins are RELA
56 transcriptional targets (Sun et al., 1993; Hoffmann et al., 2002). The pattern of
57 RELA translocation has been shown to dictate the specificity and timing of RELA
58 target gene expression, including the genes encoding I κ B α , I κ B ϵ and the
59 chemokine RANTES (Ashall et al., 2009; Lane et al., 2017). However, most studies
60 characterising RELA translocation dynamics following stimulation use
61 hyperphysiological TNF α concentrations (10 ng/ml) and exogenous RELA
62 reporters.

63 Cell shape can be a readout of a cell's signalling state and predictive of several
64 properties, including invasiveness, tumour formation and metastatic potential
65 (Thiery and Sleeman, 2006; Wu et al., 2020). We previously showed that cell shape
66 is an important regulator of RELA dynamics in breast cancer cell lines (Sero et al.,

67 2015) and RELA activity, coupled to cell shape, is predictive of breast cancer
68 progression (Sailem and Bakal, 2017). Specifically, we demonstrated that breast
69 cancer cells with mesenchymal cell shape (protrusive with low cell-cell contacts)
70 have higher RELA nuclear translocation. Because RELA activation itself promotes
71 the epithelial-to-mesenchymal transition (EMT) (Huber et al., 2004; Pires et al.,
72 2017), we provided evidence that cell shape establishes a positive feedback loop
73 that can lead to sustained RELA activation (Sero et al., 2015). Although the
74 mechanistic basis for how cell shape regulates RELA remains poorly understood,
75 studies have shown that chemically inhibiting actin or tubulin dynamics can
76 increase RELA binding to DNA and RELA-dependent gene expression (Rosette
77 and Karin, 1995; Bourgarel-Rey et al., 2001; Németh et al., 2004).

78 Despite frequent upregulation of both TNF α and RELA in PDAC tumours
79 (Weichert et al., 2007; Zhao et al., 2016), the single cell RELA translocation
80 dynamics in PDAC cells are unknown. Here, we characterised live endogenous
81 RELA translocation dynamics in single living PDAC cells from two different origins
82 and identified distinct groups of responses, including sustained, damped, and
83 unresponsive. We use Bayesian analysis to identify that inter-line and intra-line
84 differences in actin organisation are predictive of heterogeneity in RELA
85 localisation. Subsequently, small-molecule inhibition of actin and tubulin modulated
86 TNF α -mediated RELA ratios. In particular, formin and ARP2/3 inhibition
87 downregulated RELA nuclear localisation, indicating a role of actin nucleation and
88 branching in TNF α -mediated RELA translocation.

89 **Results**

90 **TNF α -induced RELA nuclear translocation dynamics is heterogenous and** 91 **sustained in MIA PaCa2 cells**

92 To study dynamic changes in RELA localisation over time, we used CRISPR-
93 CAS9 gene editing to fluorescently tag endogenous RELA at the C-terminus with
94 eGFP (abbreviated as RELA-GFP) in the human PDAC cell lines MIA PaCa2 and
95 PANC1 (Figure 1A). MIA PaCa2 and PANC1 cells are epithelial in origin and share
96 mutations common in PDAC, including KRAS and p53 mutations and homozygous
97 deletions in CDKN2A/p16 (Deer et al., 2010). We also introduced mScarlet-I to the
98 C-terminus of PCNA (Proliferating Cell Nuclear Antigen; abbreviated as PCNA-
99 Scarlet) – a processivity factor for DNA polymerase δ that functions during
100 replication – which served as a nuclear marker for segmentation and as a cell cycle
101 marker (Kurki et al., 1986; Barr et al., 2017) (Figure 1B).

102 To observe live RELA translocation dynamics in response to inflammatory
103 stimuli, we used timelapse confocal microscopy with automated image analysis to
104 track changes in RELA-GFP localisation on a single cell level in response to
105 treatment with TNF α . 0.01 ng/ml TNF α is a physiological dose relevant to both
106 healthy and malignant tissue, while 0.1 ng/ml TNF α is found in highly inflammatory
107 PDAC microenvironments (Zhao et al., 2016). 10 ng/ml TNF α was used in several
108 studies assaying RELA translocation and is included for comparison, but is
109 substantially above physiological levels (Zhao et al., 2016). RELA localisation was
110 measured using the RELA ratio: mean nuclear RELA-GFP intensity divided by
111 mean ring region RELA-GFP intensity (Figures 1C and 1D).

112 At the population level, varying TNF α levels in MIA PaCa2 led to largely
113 monophasic RELA translocation responses (Figure 2A). However, we observed
114 extensive cell-to-cell variability in RELA translocation dynamics. We collated single
115 cell RELA ratio traces from all TNF α treatments and used hierarchical clustering
116 software to identify groups of RELA translocation responses (Dobrzyński et al.,
117 2020). We identified four groups of RELA dynamics in MIA PaCa2 cells (Figures 2B
118 and 2C).

119 To profile clusters quantitatively, we detected peaks in RELA ratio tracks and
120 calculated the amplitude and time after TNF α addition to reach the first peak.
121 Clusters differed significantly in median first peak RELA ratios, ranging from 1.02
122 (Cluster M1) to 1.44 (Cluster M4). (Figure 2D). Interestingly, 32% cells from Cluster
123 M1, equivalent to 5% of all tracked MIA PaCa2 cells, maintained predominantly
124 cytoplasmic RELA (peak RELA ratio <1) following TNF α addition.

125 Across TNF α doses, MIA PaCa2 cells had a median time to first peak of 40 min,
126 which is comparable to our findings in breast epithelial cells (Sero et al., 2015).
127 However, we also observed heterogeneity in terms of the rate of RELA
128 translocation, as clusters with higher peak RELA ratio peaked at a shorter time
129 after TNF α addition (Figure 2E).

130 All TNF α doses evoked multiple RELA response classes with reproducible
131 amounts of heterogeneity. There was a trend for increasing doses of TNF α to be
132 associated with more rapid and more intense peak RELA ratios. M1 and M2
133 classes predominate at the TNF α low doses, while 10 ng/ml responses were
134 enriched for M4 and M3 classes. All four classes were observed at physiological

135 TNF α levels (0.1 ng/ml), leading to the highly heterogeneous responses (Figure
136 2F).

137 **PANC1 cells exhibit more homogeneous and damped RELA dynamics in**
138 **response to TNF α**

139 We also assayed TNF α stimulated RELA dynamics in PANC1 cells. Overall,
140 PANC1 cells had lower RELA nuclear translocation compared to the MIA PaCa2
141 cells. Moreover, 0.01 ng/ml and 0.1 ng/ml TNF α induced similar responses in
142 PANC1 cells but not in MIA PaCa2 cells (Figure 2G), indicating a higher threshold
143 before inflammation triggers a RELA response in PANC1 cells.

144 As with MIA PaCa2 cells, we identified four classes of TNF α -induced RELA
145 responses in PANC1 cells: weakly responsive (Class P1); moderately responding
146 with sustained peak RELA ratio (Class P2), or strong response with damped
147 nuclear RELA localisation (Clusters P3 and P4) (Figures 2H and 2I). 21% of cells in
148 Class P1, and 12% of all PANC1 cells, maintained cytoplasmic localisation
149 following TNF α stimulation (peak RELA ratio <1) indicating around twice as many
150 non-responsive PANC1 cells compared to MIA PaCa2 cells. PANC1 Clusters P3
151 and P4 represent a type of translocation response uncommon in MIA PaCa2 cells
152 in which RELA nuclear localisation significantly drops after peaking. Thus, in
153 contrast to MIA PaCa2 cells where many cells sustain high nuclear RELA
154 localisation, RELA activation declines following TNF α stimulation in PANC1 cells,
155 typically resulting in re-localisation to the cytoplasm within 10 hours. As negative
156 feedback signalling is a widely reported feature of RELA signalling (Hoffmann et al.,
157 2002), these data suggest that negative feedback regulation is intact in PANC1
158 cells but compromised in MIA PaCa2 cells.

159 PANC1 and MIA PaCa2 cells also differed in the proportion of cells falling into
160 each RELA translocation class, especially at physiological TNF α doses. In MIA
161 PaCa2 cells, RELA translocation dynamics exhibit a continuity of responses at
162 TNF α physiological levels (Figure 2F), as they can be grouped into all classes (M1-
163 M4). Moreover, MIA Paca2 which makes incremental responses to increased dose.
164 However, RELA responses to TNF α in PANC1 cells appear to be more 'all-or-
165 none'. RELA either responds very little at physiological doses (class P1 and P2) or
166 is 'all in' for hyperphysiological doses (class P3 and P4) (Figure 2L).

167 Strikingly, although MIA PaCa2 and PANC1 cells showed fluctuations in RELA
168 ratio over time, neither demonstrated the amplitude or regularity of periodic
169 oscillations on a single cell level observed in other cell lines (Nelson et al., 2004;
170 Tay et al., 2010; Sero et al., 2015; Zambrano et al., 2016). As oscillations are
171 driven by negative feedback in RELA signalling (Hoffmann et al., 2002), lack of
172 oscillations provides further evidence that negative feedback by I κ B α is absent in
173 MIA PaCa2 cells. Interestingly, although some form of negative feedback appears
174 to be present in PANC1 cells, the pathway parameters do not support oscillations.

175 **RELA translocations dynamics are cell cycle independent in PDAC cells**

176 Our data suggest that RELA translocation in some cells is unresponsive to
177 TNF α -stimulation (Figures 2B and 2H). As RELA nuclear translocation was
178 identified as suppressed during S-phase of the cell cycle in HeLa cells (Ankers et
179 al., 2016), we tested whether RELA translocation is cell cycle dependent in PDAC
180 cells. To this end, we used changes in the appearance and intensity of endogenous
181 PCNA-Scarlet to mark cell cycle transitions. Consistent with prior observations of
182 PCNA appearance (Kurki et al., 1986), our endogenously tagged PCNA-Scarlet

183 appeared uniform in G1, punctate during S-phase, and uniform with high intensity
184 in G2 (Figures S1A and S1B).

185 We categorised each tracked cell by cell cycle stage at the time of 0.1 ng/ml or
186 10 ng/ml TNF α addition and calculated the amplitude and timing of the first peak of
187 RELA ratio, as well as the RELA translocation cluster distribution (Figures S1C-H).
188 Broadly, we did not find differences in the time series profiles of RELA translocation
189 responses between cells in different cell cycle stages (Figures S1C and S1F). We
190 also did not find differences in the amplitude, time to RELA ratio peak, or
191 enrichment of cell cycle stages in different RELA response clusters (Figures S1D-E
192 and S1G-H). Altogether, our data indicate that cell cycle progression does not
193 underlie the observed heterogeneity in RELA translocation to TNF α in PDAC cells.

194 **Actin organisation differences are predictive of heterogeneity in TNF α -**
195 **mediated RELA localisation between and within PDAC cell lines**

196 Because the same TNF α concentration can lead to variable responses, we
197 propose there are cell-intrinsic mechanisms dictating the extent of RELA
198 translocation in PDAC cells. Having previously identified relationships between cell
199 shape and RELA localisation in breast cells (Sero et al., 2015), we hypothesised
200 that differences in actin and tubulin organisation, which lead to cell shape
201 differences, may explain differences in RELA dynamics. To test this, we expanded
202 our dataset to include images of the human immortalised PDAC cell lines MIA
203 PaCa2, PANC1, Capan1, SW1990 and PANC05.04, and the non-malignant retinal
204 epithelial line RPE1. Cell lines were treated with TNF α (1 hr) and stained for DNA,
205 RELA, F-actin and α -tubulin (Figure S2A). We used automated image analysis to
206 segment cell regions and measured 35 geometric, cytoskeletal and Hoechst

207 features, as well as RELA ratio (Figure S2B) in ~160,000 cells. We used
208 hierarchical clustering to reduce the 35 cell features to ten independent features
209 (Figure S2C). The selected features included 'Tubulin texture' which identifies
210 dense clusters of α -tubulin, as well as the ratio of 'Actin filament area' to 'Cell area'
211 which assays actin stress fibre abundance. Features were compared between cell
212 lines using principal component analysis (PCA) (Figure S3). PCA largely clustered
213 data by cell line, indicating distinct cell morphology and cytoskeletal organisation
214 between cell lines.

215 Across the five PDAC cell lines the variance of RELA ratios generally increased
216 with TNF α concentration. Cell lines also had varied sensitivity to TNF α in RELA
217 localisation (Figure 3A). Consistent with our observations of endogenously tagged
218 RELA, we confirmed that MIA PaCa2 cells have significantly higher nuclear RELA
219 localisation with increasing TNF α treatment, while PANC1 cells have only slightly
220 higher nuclear localisation in physiologically high (0.1 ng/ml) compared to
221 physiologically low (0.01 ng/ml) TNF α .

222 To identify features correlating with RELA localisation differences, we collated
223 and incorporated normalised single cell measurements for the ten independent cell
224 features into Bayesian networks. Bayesian networks are models consisting of
225 nodes, representing measured features, and arcs between nodes depicting
226 predicted dependencies based on statistical inference. Bayesian network models
227 can represent linear and non-linear relationships, direct and indirect interactions,
228 and illustrate multiple interacting nodes simultaneously (Friedman, 2004; Sachs et
229 al., 2005). We employed a hybrid class of Bayesian algorithm ('rsmx2'), which
230 uses a combination of constraint-based and score-based approaches (Scutari et
231 al., 2018).

232 To establish patterns in RELA dependencies across PDAC lines, we generated
233 Bayesian network models for each cell line for varying TNF α concentrations and
234 summarised dependencies involving RELA ratio in Figure 3B. RELA ratio had a
235 strong and consistent relationship with neighbour contact across all PDAC lines but
236 not in the non-malignant line RPE1. RELA ratio was frequently dependent on
237 cytoplasm actin intensity, cytoplasm tubulin intensity and membrane/cytoplasm
238 actin, suggesting that TNF α mediated RELA nuclear translocation is dependent on
239 cytoskeletal dynamics in PDAC cells. Conversely, nucleus roundness was
240 predicted to be dependent on RELA ratio in several contexts. Some dependencies
241 between RELA ratio and a cell feature changed with TNF α , including the
242 dependency of RELA ratio on cytoplasm tubulin mean which was more probable
243 with TNF α , while correlations between RELA ratio and cell area were more
244 probable in basal conditions.

245 To identify cell features that likely explain RELA localisation differences between
246 cell lines at high levels of inflammation, we focused on the Bayesian model for 1 hr
247 0.1 ng/ml TNF α incorporating data from all five PDAC lines (Figure 3C). The
248 features with the strongest statistical likelihood of influencing RELA localisation
249 differences between cell lines were cell area and cytoplasm actin mean, which both
250 negatively correlated with RELA ratio. These data suggest that the smaller cell area
251 and lower actin abundance of MIA PaCa2 cells compared to PANC1 cells
252 contribute to increased RELA nuclear translocation in MIA PaCa2 cells in response
253 to TNF α .

254 We assessed which features underlie heterogeneity in RELA localisation within
255 PDAC cell lines (Figure 4A-C). RELA ratio differences within both the MIA PaCa2
256 and PANC1 cell lines were predicted to depend on actin stress fibre abundance.

257 MIA PaCa2 cells showed additional dependencies on actin cytoplasm intensity and
258 actin membrane/cytoplasm intensity, which we interpret as the amount of cortical
259 actin and could reflect membrane tension, while PANC1 cells showed unique
260 dependencies of RELA localisation on tubulin abundance and nuclear roundness.
261 Overall, our data show that the relationship between RELA localisation and the
262 cytoskeleton, in particular actin networks, is cell-line specific.

263 Interestingly, neighbour contact was predicted by Bayesian modelling to
264 influence several cytoskeletal features in both MIA PaCa2 and PANC1 cells.
265 Having previously identified a negative correlation between RELA ratio and breast
266 epithelial cells (Sero et al., 2015), we tested this relationship in PDAC cells by
267 calculating the RELA ratio at each TNF α dose for cells grouped by neighbour
268 contact. RELA ratio was lower in cells with higher neighbour contacts for most
269 TNF α doses and PDAC lines, suggesting that RELA nuclear translocation is
270 contact inhibited in PDAC cells (Figure 4D).

271 **Cytoskeletal and cell shape features correlate with RELA translocation** 272 **classes**

273 Next, we tested whether relationships exist between cell geometry and
274 cytoskeleton features and the different TNF α -induced live RELA translocation
275 dynamics we observed. To do this, we took a statistical reconstructive approach.
276 We used RELA-GFP-expressing MIA PaCa2 and PANC1 cells fixed at 60 min
277 following 0.1 ng/ml TNF α treatment and stained for F-actin, α -Tubulin and DNA for
278 measurement of geometry and cytoskeletal features. We then placed each cell into
279 each of the single cell dynamics clusters identified in Figure 2, by using the mean
280 and standard deviation of RELA ratio to identify stringent ranges of RELA ratio

281 associated with each cluster at the 60 minutes time point (see methods) (Figure
282 5A).

283 T-distributed stochastic neighbour embedding (tSNE) analysis of ten
284 independent cell shape and cytoskeletal features showed that cells with the same
285 RELA translocation response profile cluster together and therefore have similar cell
286 shape and cytoskeletal organisation (Figure 5B). Features that differ between
287 RELA translocation clusters were identified by ANOVA, using all clusters (M1-M4)
288 for MIA PaCa2 cells and clusters P1-P3 for PANC1 cells, due to a lack of P4-type
289 responding cells to 0.1 ng/ml TNF α . MIA PaCa2 cells with a high number of actin
290 filaments, less cortical actin, higher cell aspect ratio (width to length) and less
291 bundled tubulin were more likely to fit a higher nuclear RELA translocation
292 response to 0.1 ng/ml TNF α (Figure 5C). Conversely, PANC1 cells with more actin
293 filaments were more likely to be unresponsive (Cluster P1) to 0.1 ng/ml TNF α ,
294 while cells with smaller cell area, higher tubulin abundance and low nucleus
295 roundness were more likely to induce RELA nuclear translocation following 0.1
296 ng/ml TNF α (Clusters P2 and P3) (Figure 5D).

297 In Figure 5E and Figure 5F, we summarised the identified relationships between
298 RELA ratio and cell features by the two statistical methods: 1) cross referencing cell
299 shape and RELA translocation response assayed by ANOVA, 2) Bayesian
300 analysis. In MIA Paca2 cells, decreased cortical actin, but increased stress fibre
301 assembly, increased cell roundness, and expansion of tubulin networks are
302 predicted to high and chronic RELA nuclear translocation. Meanwhile, PANC1 cells
303 with fewer stress fibres, decreased cell area, and distorted nuclei have higher RELA
304 nuclear translocation. However, in contrast to MIA PACA2 cells, RELA activation
305 occurs acutely and becomes suppressed in PANC1 cells. Overall, our analyses

306 show that heterogeneity in RELA translocation dynamics is linked to heterogeneity
307 in cell shape and cytoskeletal organisation in PDAC cells in a cell-line dependent
308 manner.

309 **Biochemical perturbation of the cytoskeleton modulates the effect of TNF α**
310 **on RELA translocation**

311 As cytoskeletal organisation was a strong predictor of TNF α -induced RELA
312 translocation, we tested the effect of perturbing cytoskeletal dynamics on RELA
313 localisation using small-molecules targeting tubulin, actin, myosin, or focal
314 adhesion (FA) dynamics. We ascertained doses by treating MIA PaCa2 cells with
315 concentration ranges for 24 hr, or 3 hr for SMIFH2 (Figure S4A-H).

316 To assay the effect of cytoskeleton interference on TNF α -stimulated RELA
317 translocation, we treated MIA PaCa2 and PANC1 cells with selected drug doses for
318 2 hr then simultaneously with 10 ng/ml TNF α for 1 hr. Broadly, we found that
319 inhibitors with similar mechanisms induce analogous effects on RELA translocation.
320 In MIA PaCa2 cells, targeting actin had inhibitor-specific effects on RELA
321 localisation (Figure 6A). Actin nucleation is the formation of complexes of actin
322 monomers from which actin filaments can form. CK666 inhibits the ARP2/3
323 complex – a key mediator of actin filament nucleation and branching (Mullins et al.,
324 1998), while SMIFH2 inhibits formins (Rizvi et al., 2009), which promote nucleation
325 and elongation of pre-existing actin filaments to produce long straight filaments
326 (Pruyne et al., 2002). SMIFH2, and to a lesser extent CK666, significantly
327 downregulated nuclear RELA localisation in MIA PaCa2, indicating that nucleation
328 of both branched actin and actin stress fibres function in TNF α -mediated RELA
329 nuclear translocation. Cytochalasin D, which binds to the growing end of actin

330 filaments and inhibits polymerisation (Schliwa, 1982), caused no effect on RELA
331 ratio, indicating that actin organisation, rather than actin polymerisation itself,
332 contributes to RELA nuclear translocation.

333 In MIA PaCa2 cells, inhibition of myosin/ROCK and FAK increased cell area and
334 elongation as expected but had minimal effects on actin and tubulin abundance
335 and distribution, and all increased RELA nuclear translocation. These data suggest
336 that cell contractility or focal adhesion dynamics may suppress TNF α -induced
337 RELA nuclear translocation independently of actin and tubulin dynamics.

338 Similar to MIA PaCa2 cells, actin perturbations caused reductions in RELA ratio
339 in PANC1 cells (Figure 6B), however, PANC1 cells were more sensitive to CK666
340 and cytochalasin D compared with MIA PaCa2. Myosin and FAK inhibition caused
341 milder effects on cell shape in PANC1 cells compared to MIA PaCa2, which may be
342 related to the flat/less contractile morphology of PANC1 cells observed in Figure
343 S3, and these drug groups caused non-significant RELA ratio changes in PANC1
344 cells. While targeting tubulin had no effect on RELA localisation in MIA PaCa2
345 cells, PANC1 cells were sensitive to tubulin inhibition, in particular tubulin
346 depolymerisation by vinblastine and demecolcine caused reductions in RELA ratio.
347 This supports our predictions using Bayesian modelling that RELA is dependent on
348 tubulin dynamics in PANC1 cells but not in MIA PaCa2 cells.

349 Having screened for drugs targeting the cytoskeleton that perturb RELA nuclear
350 translocation and identified SMIFH2 as a significant hit, we investigated the
351 relationship between formin dynamics and RELA activity. On the single cell level,
352 MIA PaCa2 and PANC1 cells had more cytoplasmic RELA localisation with
353 SMIFH2 and TNF α combination compared to TNF α alone, with a more significant

354 change in MIA PaCa2 cells (Figure 6C). Formin overactivation via constitutively
355 active mDia1 (CA-mDia-GFP) (Rao et al., 2013) resulted in an increase in RELA
356 ratio with TNF α in MIA PaCa2 cells, but no difference in PANC1 cells, compared to
357 TNF α alone.

358 Altogether, our data identify that actin structure and dynamics in PDAC cells
359 modulate RELA subcellular localisation, however, the precise mechanism for this is
360 different between MIA PaCa2 and PANC1 cells, as predicted by differing influences
361 by actin features on RELA ratio assessed by Bayesian analysis. RELA nuclear
362 translocation is highly dependent on nucleation of actin stress fibres in MIA PaCa2
363 cells, while RELA nuclear translocation is more dependent on nucleation of
364 branched actin in PANC1 cells (Figure 6D).

365 **Discussion**

366 RELA activity is upregulated in multiple cancers (Karin, 2009), including
367 Pancreatic Ductal Adenocarcinoma (PDAC), in which high RELA expression is
368 associated with a poor prognosis (Weichert et al., 2007). Despite the importance of
369 RELA in PDAC, RELA translocation dynamics with TNF α stimulation in PDAC cells,
370 and how these might be therapeutically manipulated, is poorly understood. Here,
371 we profiled live endogenous RELA nuclear subcellular localisation changes on the
372 single cell level in PDAC cells with varying TNF α levels. We found that PDAC cells
373 are highly sensitive to TNF α stimulation in terms of RELA nuclear translocation, as
374 the majority of MIA PaCa2 cells maintained predominantly nuclear RELA.
375 Moreover, even though PANC1 cells displayed post-stimulation damped RELA
376 translocation dynamics, a characteristic observed in cell lines of other tissue origins
377 (Nelson et al., 2004; Sero et al., 2015; Zambrano et al., 2016), other studies

378 reported more rapid cytoplasmic RELA localisation (within 2 hours of TNF α
379 treatment) compared to PANC1 cells, where RELA ratio falls below 1 between 6-8
380 hours after TNF α treatment (clusters P3 and P4). Nonetheless, we identified
381 similarities in the timing of RELA translocation with previous reports, with peak
382 RELA nuclear localisation at a median of 40 min following TNF α treatment for MIA
383 PaCa2 cells and 50 min for PANC1 cells.

384 Notably, we observed extensive heterogeneity in single cell RELA responses
385 within PDAC cell lines, which could be categorised into distinct classes of
386 dynamics. We used Bayesian modelling of five PDAC lines as an unbiased and
387 high dimensional approach to determine whether descriptors of cell shape and the
388 cytoskeleton correlate with RELA localisation. We previously used Bayesian
389 modelling to show that RELA localisation in a panel of breast cells is strongly
390 dependent on neighbour contact, cell area, and protrusiveness in the presence and
391 absence of TNF α (Sero et al., 2015). In the present study, we extended our
392 analysis to include measurements of actin and tubulin organisation and found that
393 differences in cytoplasmic actin intensity, as well as measures of actin localisation
394 (cortical versus cytoplasmic actin), correlated with RELA ratio differences within
395 and between PDAC cell lines.

396 We tested the effect of modulating the cytoskeleton and cell shape, using small-
397 molecule inhibitors, on RELA subcellular localisation with TNF α in PDAC cells and
398 identified that perturbing actin dynamics downregulates RELA nuclear localisation.
399 However, RELA nuclear localisation was more perturbed by formin inhibition in MIA
400 PaCa2 cells and by ARP2/3 inhibition in PANC1 cells, suggesting differing
401 contributions of actin stress fibres and branching to the overall organisation of actin
402 and subsequently cell shape in these two cell lines, in addition to differing

403 influences of the nucleation of actin branches and stress fibres on RELA nuclear
404 translocation. The higher impact of inhibition of actin polymerisation by cytochalasin
405 D on RELA translocation in PANC1 cells compared to MIA PaCa2 cells suggests
406 that actin structures are more dynamic in PANC1 cells. As the serum response
407 factor coactivator MAL is sequestered in the cytoplasm by monomeric actin and
408 then released when actin is incorporated into F-actin filaments (Miralles et al.,
409 2003), we hypothesised that actin may regulate RELA in a similar manner.
410 However, the insufficiency of cytochalasin D to affect RELA nuclear translocation in
411 MIA PaCa2 cells suggests that actin polymerisation alone is insufficient to regulate
412 RELA localisation.

413 Furthermore, the relationship between neighbour contact, actin remodelling, and
414 RELA translocation remains a source for further study. As we observed a negative
415 correlation between neighbour contact and RELA, as well as several dependencies
416 of actin features on neighbour contact predicted by Bayesian modelling in Figure
417 4B and C, we suggest that neighbour contact may regulate RELA by altering actin
418 structure. This may represent a mechanism used by PDAC cells to sense the
419 environment – and whether in contact with extracellular matrix or other cells – to
420 modulate RELA activity accordingly. Mechanistically, one route which may be
421 mediating transduction of contact information is through beta or p120 (delta)
422 catenin proteins, which regulates the stability of adherens junctions. p120 inhibits
423 RELA activity as p120 null epidermal cells have activated nuclear RELA and p120
424 null mice have chronic inflammation (Perez-Moreno et al., 2006).

425 We hypothesise that the cell signalling between actin dynamics and RELA likely
426 involves RhoGTPases, which are central regulators of actin previously linked to the
427 NF- κ B pathway (Tong and Tergaonkar, 2014). For instance, NIH-T3 cells with

428 dominant negative mutant CDC42 or RhoA, but not Rac-1, have significantly lower
429 NF- κ B transcriptional activity with TNF α compared to their wildtype counterparts
430 (Perona et al., 1997). We have also shown that RELA regulation by cell shape and
431 neighbour contact is regulated by RhoA in breast cells (Sero et al., 2015). It would
432 therefore be interesting to screen for RhoGTPases regulating actin nucleation and
433 branching and RELA translocation in PDAC.

434 Potential mechanisms for actin regulation of RELA may also be hypothesised
435 from research on the mechanosensitive transcriptional regulator YAP. For example,
436 YAP nuclear translocation is upregulated when forces are applied to ECM
437 adhesions, which stretch nuclear pores via the actin cytoskeleton (Elosegui-Artola
438 et al., 2017). Actin remodelling may therefore affect RELA localisation by reshaping
439 nuclear pores, which could impact RELA nuclear import or export.

440 Targeting RELA nuclear translocation is an attractive therapeutic strategy, as
441 RELA activity may promote a high-inflammatory PDAC tumour microenvironment
442 through regulation of cytokine production (Ling et al., 2012; Steele et al., 2013), in
443 addition to regulating cell processes that underlie PDAC oncogenesis (Melisi et al.,
444 2009) and therapeutic resistance (Arlt et al., 2003). Our data suggest that RELA
445 activation may be fine-tuned in PDAC by targeting both the cytoskeleton and
446 inflammation. For instance, anti-TNF α therapy previously determined ineffective in
447 advanced pancreatic patients (Wu et al., 2013) may be effective when combined
448 with therapy targeting the cytoskeleton. Moreover, tissue specific and patient
449 specific actin or tubulin dynamics may present a therapeutic opportunity.

450 Although compounds directly targeting actin are toxic and unusable in the clinic,
451 there is potential to target actin-regulating proteins (Bryce et al., 2019). Ability to

452 target actin in cancer cells selectively may be enabled by tissue specificity and
453 isoform diversity of ARP2/3 complex components (Abella et al., 2016; Jay et al.,
454 2000), or upregulation of the Tpm3.1 isoform of the actin binding protein
455 Tropomyosin in cancer cells (Stehn et al., 2013).

456 **Acknowledgements**

457 We gratefully acknowledge funding for this work by Cancer Research UK, awarded
458 to F.B. (S_3567). We thank Andrea Brundin for assistance with single cell tracking
459 and Lucas Dent for helpful comments on the manuscript.

460 **Author Contributions**

461 F.B., J.E.S., and C.B. conceived the study. F.B. performed the experiments and
462 image analysis. F.B. wrote the manuscript with support and discussion from C.B,
463 J.E.S. and L.D..

464 **Declaration of Interests**

465 The authors declare no competing interests.

466

467 **Figure Titles and Legends**

468 **Figure 1: Generation of PDAC lines with endogenous RELA-GFP and PCNA-** 469 **Scarlet**

470 (A-B) Schematic of CRISPR-CAS9 gRNA and homology constructs generated for
471 endogenous C-terminal tagging of RELA and PCNA with fluorescent proteins. (C)
472 Confocal microscopy of endogenous RELA-GFP and PCNA-Scarlet in MIA PaCa2
473 and PANC1 cells in control or 0.1 ng/ml TNF α conditions. (D) Example of
474 automated segmentation of nuclear and ring regions using PCNA-Scarlet. RELA
475 localisation is measured by the ratio of RELA-GFP intensity in the nucleus to the
476 ring region. RELA ratios are calculated for single cells tracked prior to and following
477 TNF α treatment.

478 **Figure 2: Endogenous RELA translocation dynamics in response to TNF α in** 479 **PDAC cells**

480 (A) Average RELA-GFP translocation responses in MIA PaCa2 cells per TNF α
481 dose (0.01 ng/ml, 0.1 ng/ml and 10 ng/ml) from 120 min prior to until 600 min
482 following TNF α treatment. $n = 50-60$ tracked cells per TNF α dose for each of two
483 biological repeats. Lines denote the mean and grey ribbons represent the standard
484 error of the mean (SEM). (B-C) Hierarchical clustering of RELA ratio tracks of MIA
485 PaCa2 collated from all TNF α treatments (0.01 ng/ml, 0.1 ng/ml and 10 ng/ml) into
486 four groups using Time Course Inspector in R with the 'Ward D2' linkage method
487 and 'Manhattan' dissimilarity measure. $n = 50-60$ tracked cells per TNF α dose for
488 each of two biological repeats. Heat map is coloured according to the RELA ratio
489 and each row represents an individual tracked cell. Individual tracks per cluster are
490 shown to the left. Clusters from MIA PaCa2 cells are prefixed with 'M'. (D)

491 Amplitude and (E) Time of first RELA-GFP ratio peak in individual MIA PaCa2 cells
492 per cluster M1-M4. Boxplots show median and interquartile range. M = median per
493 cluster. σ = standard deviation per cluster. (F) Proportion of MIA PaCa2 tracks per
494 TNF α treatment in each cluster M1-M4. (G) Average RELA-GFP translocation
495 responses in PANC1 cells per TNF α dose. $n = 50-60$ tracked cells per TNF α dose.
496 (H-I) Hierarchical clustering of RELA ratio tracks for PANC1 cells collated from all
497 TNF α treatments. Clusters from PANC1 cells are prefixed with 'P'. (J) Amplitude
498 and (K) Time of first RELA-GFP ratio peak in individual PANC1 cells per cluster P1-
499 P4. Boxplots show median and interquartile range. M = median per cluster. σ =
500 standard deviation per cluster. (L) Proportion of PANC1 tracks per TNF α treatment
501 in each cluster P1-P4.

502 **Figure 3: Heterogeneity in cell area and actin abundance are predictive of cell**
503 **line differences in TNF α mediated RELA localisation**

504 (A) Single cell RELA ratio distributions by immunofluorescence and automated
505 image analysis. (B) Dependencies involving RELA ratio in Bayesian network
506 models generated with single cell data for individual treatments or cell lines, or for
507 all PDAC cell lines collated (top row per cell feature section). Purple represents a
508 dependency of RELA on the cell feature in the Bayesian network model. Orange
509 represents a dependency of a cell feature on RELA. Dependency strengths are
510 calculated as $\log_2(|\text{arc strength}|)$, multiplied by -1 for dependencies of cell features
511 on RELA ratio. (C) Bayesian networks model incorporating data from all PDAC
512 lines (RPE1 excluded) treated with 1 hr 0.1 ng/ml TNF α . Values next to arcs
513 represent the strength of the probabilistic relationship expressed by the arc (arc
514 strength). Arcs leading to or away from RELA Ratio are dashed. Top right:

515 schematic of construction of the Bayesian network model. Bottom right: single cell
516 measurements for cell area, cytoplasmic actin intensity, and RELA ratio.

517 **Figure 4: Bayesian network analysis identifies relationships between cell**
518 **shape and cytoskeletal features with RELA localisation within PDAC**
519 **populations**

520 (A-C) Bayesian networks models were generated each incorporating single cell
521 data from a single PDAC cell line. (D) Mean RELA ratio +/- standard deviation
522 against (rounded) neighbour contact by treatment.

523 **Figure 5: Cytoskeletal and cell shape features correlate with RELA**
524 **translocation response profiles**

525 (A) Schematic illustrating method for RELA translocation response cluster
526 classification. RELA ratio limits per cluster are defined by the mean and number (n)
527 of standard deviations from the mean, calculated from live imaged cells. Cells are
528 independently sorted into clusters based on RELA ratio at the same timepoint after
529 0.1 ng/ml TNF α addition. Below are cluster prediction accuracies calculated as the
530 percentage of clustered cells tracked through live imaging with the correct cluster
531 identified using the model limits. (B) t-SNE analysis of MIA PaCa2 and PANC1 cells
532 by RELA translocation cluster separated by well averages of the cell shape and
533 cytoskeletal features used for Bayesian analysis, excluding Neighbour Contact. (C-
534 D) Single cell data for four measured cell features with high statistical significance
535 by ANOVA between RELA translocation clusters. Bars show mean +/- SD. (E)
536 Summary of identified relationships between RELA ratio and cell features by cross
537 referencing cell shape and RELA translocation clusters (tested by ANOVA) and
538 independently by Bayesian analysis. (F) Schematic summarising identified

539 relationships between cell shape and cytoskeletal features with RELA translocation
540 response to TNF α . MIA PaCa2 cells with more actin stress fibres, low cortical actin,
541 low cell aspect ratio, and more spread tubulin are more likely to have high nuclear
542 RELA translocation in response to 0.1 ng/ml TNF α . PANC1 cells can be
543 unresponsive or responsive to 0.1 ng/ml TNF α , with responsiveness correlated to
544 actin stress fibre and tubulin abundance, as well as nucleus roundness and cell
545 area.

546 **Figure 6: Modulation of TNF α -mediated RELA translocation by cytoskeletal**
547 **perturbation**

548 (A-B) Fold-changes for cell shape and cytoskeletal measurements following 3 hr
549 drug treatment normalised to the DMSO control. Below are the corresponding fold-
550 changes for RELA ratio (10 ng/ml TNF α /no TNF) normalised to the DMSO control.
551 Data shown for technical replicates/well averages (two per $n = 3$ biological
552 repeats). PTX = paclitaxel; Noc = nocodazole; Dem = Demecolcine; Cyto D =
553 Cytochalasin D; Blebb = Blebbistatin; PF228 = PF573228. (C) Single cell RELA
554 ratios in MIA PaCa2 and PANC1 cells treated with 0.1 ng/ml TNF α , with SMIFH2
555 treatment or 24 hr transfection with CA-mDia1-GFP (constitutively active mDia1).
556 Representative images per cell line and condition are shown. (D) RELA nuclear
557 translocation is dependent on actin structure in PDAC cells, with a higher
558 dependency on the nucleation of stress fibres in MIA PaCa2 cells and on the
559 nucleation of branched actin in PANC1.

560

561 **Materials and Methods**

562 Further information and requests for resources should be directed to and will be
563 fulfilled by the Lead Contact, Francesca Butera (francesca.butera@icr.ac.uk).

564 *Cell Line and Cell Culture*

565 Cell lines were maintained at 37°C and 5% CO₂ in Dulbecco's Modified Eagle
566 Medium (DMEM; Gibco) supplemented with 10% heat-inactivated Fetal Bovine
567 Serum (Sigma) and 1% Penicillin/Streptomycin (Gibco).

568 *Generation of cell lines with fluorescently tagged RELA and PCNA by CRISPR- 569 CAS9*

570 RELA and PCNA were tagged endogenously at each C-terminus using CRISPR-
571 mediated gene editing in MIA PaCa2 and PANC1 cells. RELA was tagged with
572 enhanced GFP (Zhang et al., 1996) and PCNA was tagged with mScarlet-I (Bindels
573 et al., 2017), abbreviated throughout this manuscript as RELA-GFP and PCNA-
574 Scarlet respectively. RELA-GFP was first introduced into wildtype cell lines then
575 PCNA-mScarlet was added to validated RELA-GFP clones.

576 Homology constructs were generated by extracting the region around the stop
577 codon of each gene by PCR. The product was used as a template to amplify the
578 left homology arm (LHA) and right homology arm (RHA) by PCR. PCRs were
579 carried out using High-Fidelity Q5 DNA Polymerase (NEB) according to the
580 manufacturer's protocol. The RHA contains a mutation corresponding to the gRNA
581 PAM site to prevent repeat targeting by the Cas9 nuclease. Primers used to amplify
582 the homology arms included overlaps for 1) a DNA cassette encoding a linker
583 protein, the fluorescent protein, and antibiotic resistance (kindly donated by Francis

584 Barr); 2) the pBluescript II SK (-) vector (Agilent) following EcoRV digestion. The
585 final homology construct was generated from the four DNA oligos by Gibson
586 assembly using the NEB Gibson Assembly Master Mix and according to the NEB
587 protocol.

588 gRNA oligos were designed using CRISPR.mit.edu. Forward and reverse oligos
589 were phosphorylated, annealed and ligated into a BbsI-digested pX330 U6
590 Chimeric hSpCas9 plasmid, gifted from Feng Zhang (Cong et al., 2013).

591 Cells were transfected with homology and gRNA constructs using Lipofectamine
592 2000 (ThermoFisher) according to the manufacturer's protocol. Cells were
593 expanded and selected for antibiotic resistance for three weeks. FP-positive cells
594 were selected using FACS and sorted into single cells per well in 96-well plates and
595 clones were expanded and tested for FP presence using Western blotting. The C-
596 terminus of the RELA and PCNA genes of genomic DNA from the selected clones
597 was amplified and sequenced to confirm the presence of the linker and eGFP or
598 mScarlet DNA.

599 *Cell seeding and treatment for fixed image analysis*

600 Cells were seeded at a density of 1,000 cells per well in 384-well plates unless
601 otherwise specified.

602 For comparison of cell shape and cytoskeletal features in the five PDAC and RPE1
603 cell lines, cells were fixed 2 days after seeding, including 1 hr TNF α treatment. The
604 experiment was carried out with three times (biological repeats) in total, each with
605 four technical replicates (wells) per condition.

606 *TNF α treatment*

607 Cells were treated with human recombinant TNF α diluted in complete medium at a
608 final concentration of 0.1 ng/ml, or 1 ng/ml and 10 ng/ml when specified. TNF α
609 sourced from Sino Biological was diluted in water and used to treat the panel of
610 PDAC lines for Bayesian analysis (Figure 3). Due to lack of availability, TNF α was
611 sourced from R&D Systems and diluted in 0.1% BSA/PBS for all other experiments.

612 *Immunofluorescence*

613 Cells were fixed with warm formaldehyde (FA) dissolved in PBS at a final
614 concentration of 4% for 15 min at 37°C then washed three times with PBS. Cells
615 were permeabilised in 0.2% TritonX-100 (Sigma Aldrich) dissolved in PBS for 10
616 min and blocked in 2% BSA/PBS for 1 hr at RT (room temperature). Cells were
617 stained with 10 μ g/ml Hoechst (Sigma Aldrich) in PBS (1:1,000) for 15 minutes,
618 washed three times and left in PBS/azide before imaging.

619 Cells were incubated with primary antibodies for 2 hr at RT or overnight at 4 °C,
620 washed three times with PBS, and incubated with secondary antibodies for 90 min
621 at RT.

622 Primary antibodies used were rabbit anti-p65/RELA NF- κ B (Abcam; 1:500), rat anti-
623 α -tubulin (Bio-Rad; 1:1000), and pFAK Tyr397 (Invitrogen; 1:250).

624 Cells were incubated with secondary antibodies for 90 min at RT. Secondary
625 antibodies used were Alexa 488/568/647 goat anti-rabbit/mouse/rat IgG
626 (Invitrogen).

627 For F-actin staining, cells were incubated with Alexa-568 phalloidin (Invitrogen;
628 1:1000) for 90 min simultaneously with secondary antibodies.

629 *Imaging and automated analysis of fixed cells*

630 A minimum of 21 fields of view per well were imaged using the PerkinElmer Opera
631 confocal microscope using a 20x air objective. Image analysis was performed using
632 custom image analysis scripts created and executed on PerkinElmer's Columbus
633 2.6.0 software platform. Scripts detected and segmented individual nuclei using
634 Hoechst and the cytoplasm using Tubulin, or RELA when Tubulin is not included in
635 the staining set. Cells touching the image border are filtered out and neighbour
636 contact (% cell border touching another cell) for each remaining cell is calculated.
637 The nuclear region is reduced by 1 px from the nuclear outer border from Hoechst
638 segmentation and the ring region is set as the area 2 px to 6 px outside of the
639 nuclear outer border. Intensities of all stains are calculated in all segmented regions
640 on a single-cell level. A total of 32 geometric, cytoskeletal and Hoechst features
641 were measured in addition to measurements of RELA/RELA-GFP. RELA Ratio is
642 calculated by dividing the mean nuclear intensity of RELA/RELA-GFP by the mean
643 ring region intensity of RELA/RELA-GFP. Texture features were calculated using
644 SER methods with region normalisation. Bright and Spot textures were smoothed
645 to a kernel of 4px to detect large patches (bundles) of actin/tubulin. Ridge texture
646 was non-smoothed to detect sharp ridges (filaments) of actin/tubulin.
647 Elongatedness was calculated as $((2 * \text{Cell Length})^2 / \text{Cell Area})$. Actin Filament Area
648 was measured using Columbus's 'Find Spots' function applied to the actin channel.
649 Neighbour contact was calculated using an inbuilt Columbus algorithm calculating
650 the percentage of a cell's border in contact with other cell borders. Grouped
651 neighbour contact measurements were generated from non-normalised data
652 rounded to the nearest multiple of ten.

653 *Live cell imaging and analysis*

654 MIA PaCa2 RELA-GFP PCNA-Scarlet and PANC1 RELA-GFP PCNA-Scarlet cells
655 were seeded (1,000 cells/well) in a 384-well plate one day prior to imaging. 4 fields
656 per well were imaged at 10 min intervals using the Opera QEHS imaging system
657 with a 20x air objective and an environmental control chamber set to 80% humidity,
658 5% CO₂ and 37°C. Cells were imaged for 2 hr prior to and 48 hr following TNF α
659 addition. Nuclear and ring region measurements of RELA and PCNA were carried
660 out using Nuclitrack software (Cooper et al., 2017), with 50-60 cells tracked per
661 treatment, cell line and biological repeat ($n = 2$). Cells were tracked for only 10 hr
662 following TNF α treatment while the total 48 hr imaging period was used to ascertain
663 cell fate (division or death).

664 Intensity measurements in the second biological repeat were normalised to the first
665 based on control (BSA/PBS) well measurements (TNF α absence) to account for
666 photobleaching and laser power changes. Each biological repeat consisted of eight
667 technical (well) replicates per cell line and treatment.

668 For each cell line, tracks from all treatments and biological repeats were collated
669 and trimmed to 120 min prior to until 600 min following TNF α treatment then
670 clustered using Time Course Inspector (Dobrzyński et al., 2020) in R, with Ward D2
671 linkage and the Manhattan dissimilarity measure.

672 RELA ratio peaks were detected in Excel as RELA ratios fitting either of two
673 criteria: 1) more than 0.02 above both of the average RELA ratio of the previous
674 two time points and the average RELA ratio of the following three timepoints; 2)
675 greater than 1 and is the maximum RELA ratio in the surrounding 40 min window,
676 and more than 0.01 above the average RELA ratio of the previous two time points

677 and the average RELA ratio of the following two timepoints. The ‘first peak’ is the
678 earliest occurring peak following TNF α addition.

679 *Cytoskeletal Drug Treatments*

680 2,000 MIA PaCa2 RELA-GFP cells/well were seeded in 384-well plates and treated
681 the next day with the following drugs for 24 hr without TNF α at the specified dose
682 ranges: Paclitaxel (6.25-200nM; Sigma), Vinblastine (3.125-100nM; Sigma),
683 Nocodazole (12.5-400nM; Sigma), Demecolcine (6.25-200nM; Sigma),
684 Cytochalasin D (0.125-4 μ M; Sigma), CK666 (12.5-400 μ M; Sigma), H1152 (1.25-
685 40 μ M; Tocris), Blebbistatin (1.25-40 μ M; Sigma), PF573228 (0.625-20 μ M; Tocris),
686 and Defactinib (0.625-20 μ M; Selleckchem). Cells were treated with SMIFH2
687 (3.125-100 μ M; Abcam) for only 3 hr due to reported cycles of de- and re-
688 polymerisation of 4-8 hr and inefficacy after 16 hr (Isogai et al., 2015). Ranges were
689 selected according to literature and manufacturers’ recommendations. Doses for
690 further analysis were selected based on the observed effect on the cytoskeletal
691 target and cell morphology, as quantified in Figure S4. Doses for H1152 and
692 blebbistatin were based on cell spreading, measured as cell elongatedness, as a
693 proxy of myosin inhibition (Figure S4D).

694 MIA PaCa2 and PANC1 RELA-GFP cells were seeded at 2,000 cells/well in 384-
695 well plates and treated the following day with selected doses of the small-molecule
696 inhibitors for 2 hr plus additional 1 hr co-incubation with 10 ng/ml TNF α (or DMEM
697 control) prior to fixation. $n = 3$ biological repeats. Cell feature measurements were
698 calculated as fold changes to controls (DMSO and BSA/PBS) then Z-scored across
699 TNF α treatments and cytoskeletal drugs by cell line. RELA ratios were calculated

700 as fold changes to the TNF α and cytoskeletal drug control then calculated as Z-
701 scores across all TNF α treatments by cell line.

702 *Constitutive activation of mDia1*

703 3,000 wildtype MIA PaCa2 or PANC1 cells were seeded in 100 μ l DMEM per well in
704 a PerkinElmer Ultra 96 well plate. The following day, cells were transfected with
705 GFP-CA-mDia1 using Effectene (Qiagen) according to the manufacturer's protocol.
706 Cells were fixed the following day with control (BSA/PBS) or TNF α treatment,
707 stained for RELA by immunofluorescence and with phalloidin 568 and Hoechst,
708 then imaged on a confocal microscope. GFP-positive cells were analysed using
709 CellProfiler.

710 *Quantification and Statistical Analysis*

711 To analyse cell-to-cell differences in the 35 geometric, cytoskeletal and Hoechst
712 features within and between PDAC and RPE1 cell lines, single cell and well (mean)
713 data were collated from all cell lines and treatments from three biological repeats.
714 Features were normalised to the mean across all treatments and cell lines for each
715 biological repeat. Features were reduced for Bayesian analysis by clustering
716 normalised single cell measurements into ten clusters using the 'ComplexHeatmap'
717 package in R (Gu et al., 2016), clustering by the Spearman's Rank coefficient with
718 average linkage, as shown in Figure S2. Bayesian network models and arc
719 strengths were generated in R using normalised single cell data for the ten reduced
720 features via the 'bnlearn' R package (rsmax2 method) (Scutari, 2010). This
721 algorithm depicts unidirectional arcs, so reverse relationships can exist but are not
722 as statistically likely as the directional relationships indicated.

723 MIA PaCa2 and PANC1 RELA-GFP cells fixed after 1 hr 0.1 ng/ml TNF α were
724 allocated to RELA translocation clusters based on RELA ratio, using the mean
725 RELA ratio +/- 0.6*standard deviation for live tracked cells at 60 min for each RELA
726 translocation cluster (M1-M4 and P1-P4) to define RELA ratio limits per cluster.
727 Fixed cells were stained for actin and tubulin and Z-scores for the ten independent
728 cytoskeletal and cell shape features used in Bayesian analysis were calculated by
729 cell line. t-SNE analysis was carried out in R (“Rtsne” package) using Z-score data.
730 Statistical difference between RELA translocation clusters for each cell feature by
731 cell line were identified by ANOVA.

732 Z-scores in Figure S3 were calculated per technical replicate using the mean and
733 standard deviation for control measurements for each feature across all lines for
734 each biological repeat ($n = 3$). Mean Z-scores per feature and cell line were
735 calculated by averaging Z-scores for technical replicates across all biological
736 repeats.

737 Statistical tests were carried out using the ‘Rstatix’ package in R. Principal
738 Component Analysis (PCA) was carried out in R using the inbuilt ‘prcomp’ function
739 using Z-score data. Graphs were generated in R using the ‘ggplot’ package
740 (Wickham, 2016).

741 **Supplemental Figure Legends**

742 **Figure S1: TNF α -induced nuclear RELA translocation is cell cycle** 743 **independent**

744 (A-B) Live imaging traces of endogenous PCNA-Scarlet and RELA ratio from
745 during cell division across the cell cycle until the next division in a single

746 representative untreated (A) MIA PaCa2 cell (B) PANC1 cell. Images taken at 10
747 min intervals. Nuclear PCNA-Scarlet (floored mean) and nuclear and ring region
748 RELA-GFP measurements were calculated in Nuclitrack software. Cell cycle stage
749 transitions based on PCNA intensity and appearance changes are marked with
750 dashed lines. Images of PCNA-Scarlet corresponding to the tracked cell are on the
751 right of each trace. (C) Single cell RELA ratio tracks for MIA PaCa2 cells
752 categorised by cell cycle stage at the time of TNF α addition, based on PCNA-
753 Scarlet intensity and appearance. (D) Single cell measurements for MIA PaCa2
754 cells of the RELA ratio at first peak (amplitude) and time to first peak per cell cycle
755 stage and TNF α dose. Boxplots show median and interquartile range. (E)
756 Proportion of RELA ratio tracks from MIA PaCa2 cells in each RELA translocation
757 cluster grouped by cell cycle stage at the time of TNF α addition calculated
758 separately for 0.1 ng/ml or 10 ng/ml TNF α treatment. (F) Cell cycle stage
759 categorised single cells tracks for PANC1 cells. (G) Single cell measurements of
760 RELA ratio at first peak (amplitude) and time to first peak per cell cycle stage and
761 TNF α dose for PANC1 cells. (H) Proportion of RELA ratio tracks from each PANC1
762 RELA translocation cluster grouped by cell cycle stage.

763 **Figure S2: Automated image analysis and independent cell feature selection**

764 (A) Staining by immunofluorescence (α -tubulin and RELA) and dyes marking DNA
765 (Hoechst) and F-actin (phalloidin). Cell regions were segmented using Hoechst and
766 α -Tubulin stains and features were measured in these regions using the four stains.
767 (B) RELA ratio is calculated by dividing RELA intensity in the nucleus by RELA
768 intensity in the ring region (region around nucleus in cytoplasm). (C) Hierarchical
769 clustering of 35 normalised cell features (excluding RELA measurements)

770 measured in five PDAC cell lines and RPE1. Independent features selected (one
771 per cluster) are highlighted in the dendrogram and displayed in images beside.

772 **Figure S3: Morphological diversity of PDAC cell lines**

773 Principal Component Analysis (PCA) of the ten reduced features used in Bayesian
774 analysis for five PDAC cell lines and RPE1 using two principal components.
775 Overlaid is a biplot (arrows) denoting the absolute contribution of each cell
776 feature to the two PCs. Circles represent technical replicates (four technical
777 replicates for each of three biological repeats). Horizontal bar graphs for individual
778 cell lines show mean Z-scores for each feature, calculated across the six cell lines
779 to compare differences in each feature between the cell lines. Z-scores were
780 calculated using the mean and standard deviation for control measurements across
781 all lines for each biological repeat. Displayed is the mean Z score across biological
782 repeats. Images for each cell line show Hoechst, phalloidin (F-actin), α -tubulin and
783 RELA staining by immunofluorescence.

784 **Figure S4: Dose responses of MIA PaCa2 cells to drugs targeting the** 785 **cytoskeleton**

786 (A-G) Dose responses of cytoskeleton-targeting drugs and representative images
787 of MIA PaCa2 cells (absence of TNF α). $n =$ four technical replicates per drug dose.
788 (H) Cytoplasm actin intensity (y-axis), Elongatedness (point size) and cytoplasm
789 tubulin intensity (point colour) of cells treated with selected drug concentrations in
790 the presence or absence of 1 hr 0.1 ng/ml TNF α . All measurements are normalised
791 to the DMSO control for each cell line and TNF α dose (0 or 0.1). Points show two
792 technical (well) replicates for three biological repeats per treatment combination.

793 **References**

- 794 Abella, J.V.G., Galloni, C., Pernier, J., Barry, D.J., Kjær, S., Carlier, M.-F., and
795 Way, M. (2016). Isoform diversity in the Arp2/3 complex determines actin filament
796 dynamics. *Nat Cell Biol* 18, 76–86.
- 797 Ankers, J.M., Awais, R., Jones, N.A., Boyd, J., Ryan, S., Adamson, A.D., Harper,
798 C.V., Bridge, L., Spiller, D.G., Jackson, D.A., et al. (2016). Dynamic NF- κ B and E2F
799 interactions control the priority and timing of inflammatory signalling and cell
800 proliferation. *ELife* 5, e10473.
- 801 Arlt, A., Gehrz, A., Mürköster, S., Vorndamm, J., Kruse, M.-L., Fölsch, U.R., and
802 Schäfer, H. (2003). Role of NF- κ B and Akt/PI3K in the resistance of pancreatic
803 carcinoma cell lines against gemcitabine-induced cell death. *Oncogene* 22, 3243–
804 3251.
- 805 Ashall, L., Horton, C.A., Nelson, D.E., Paszek, P., Harper, C.V., Sillitoe, K., Ryan,
806 S., Spiller, D.G., Unitt, J.F., Broomhead, D.S., et al. (2009). Pulsatile stimulation
807 determines timing and specificity of NF- κ B-dependent transcription. *Science* 324,
808 242–246.
- 809 Barr, A.R., Cooper, S., Heldt, F.S., Butera, F., Stoy, H., Mansfeld, J., Novák, B.,
810 and Bakal, C. (2017). DNA damage during S-phase mediates the proliferation-
811 quiescence decision in the subsequent G1 via p21 expression. *Nature*
812 *Communications* 8, 1–17.
- 813 Bindels, D.S., Haarbosch, L., van Weeren, L., Postma, M., Wiese, K.E., Mastop,
814 M., Aumonier, S., Gotthard, G., Royant, A., Hink, M.A., et al. (2017). mScarlet: a
815 bright monomeric red fluorescent protein for cellular imaging. *Nature Methods* 14,
816 53–56.
- 817 Bourgarel-Rey, V., Vallee, S., Rimet, O., Champion, S., Braguer, D., Desobry, A.,
818 Briand, C., and Barra, Y. (2001). Involvement of nuclear factor kappaB in c-Myc
819 induction by tubulin polymerization inhibitors. *Mol. Pharmacol.* 59, 1165–1170.
- 820 Bryce, N.S., Hardeman, E.C., Gunning, P.W., and Lock, J.G. (2019). Chemical
821 biology approaches targeting the actin cytoskeleton through phenotypic screening.
822 *Current Opinion in Chemical Biology* 51, 40–47.
- 823 Cong, L., Ran, F.A., Cox, D., Lin, S., Barretto, R., Habib, N., Hsu, P.D., Wu, X.,
824 Jiang, W., Marraffini, L.A., et al. (2013). Multiplex genome engineering using
825 CRISPR/Cas systems. *Science* 339, 819–823.
- 826 Cooper, S., Barr, A.R., Glen, R., and Bakal, C. (2017). NucliTrack: an integrated
827 nuclei tracking application. *Bioinformatics* 33, 3320–3322.
- 828 Deer, E.L., Gonzalez-Hernandez, J., Coursen, J.D., Shea, J.E., Ngatia, J., Scaife,
829 C.L., Firpo, M.A., and Mulvihill, S.J. (2010). Phenotype and Genotype of Pancreatic
830 Cancer Cell Lines. *Pancreas* 39, 425–435.

- 831 DiDonato, J.A., Hayakawa, M., Rothwarf, D.M., Zandi, E., and Karin, M. (1997). A
832 cytokine-responsive I κ B kinase that activates the transcription factor NF- κ B. *Nature*
833 *388*, 548–554.
- 834 Dobrzyński, M., Jacques, M.-A., and Pertz, O. (2020). Mining single-cell time-series
835 datasets with Time Course Inspector. *Bioinformatics* *36*, 1968–1969.
- 836 Elosegui-Artola, A., Andreu, I., Beedle, A.E.M., Lezamiz, A., Uroz, M., Kosmalka,
837 A.J., Oria, R., Kechagia, J.Z., Rico-Lastres, P., Le Roux, A.-L., et al. (2017). Force
838 Triggers YAP Nuclear Entry by Regulating Transport across Nuclear Pores. *Cell*
839 *171*, 1397-1410.e14.
- 840 Friedman, N. (2004). Inferring Cellular Networks Using Probabilistic Graphical
841 Models. *Science* *303*, 799–805.
- 842 Ghosh, S., May, M.J., and Kopp, E.B. (1998). NF- κ B and Rel Proteins:
843 Evolutionarily Conserved Mediators of Immune Responses. *Annual Review of*
844 *Immunology* *16*, 225–260.
- 845 Gu, Z., Eils, R., and Schlesner, M. (2016). Complex heatmaps reveal patterns and
846 correlations in multidimensional genomic data. *Bioinformatics* *32*, 2847–2849.
- 847 Hayden, M.S., West, A.P., and Ghosh, S. (2006). NF- κ B and the immune response.
848 *Oncogene* *25*, 6758–6780.
- 849 Hoffmann, A., Levchenko, A., Scott, M.L., and Baltimore, D. (2002). The I κ B-NF- κ B
850 Signaling Module: Temporal Control and Selective Gene Activation. *Science* *298*,
851 1241–1245.
- 852 Huber, M.A., Azoitei, N., Baumann, B., Grünert, S., Sommer, A., Pehamberger, H.,
853 Kraut, N., Beug, H., and Wirth, T. (2004). NF- κ B is essential for epithelial-
854 mesenchymal transition and metastasis in a model of breast cancer progression. *J*
855 *Clin Invest* *114*, 569–581.
- 856 Isogai, T., van der Kammen, R., and Innocenti, M. (2015). SMIFH2 has effects on
857 Formins and p53 that perturb the cell cytoskeleton. *Scientific Reports* *5*, 9802.
- 858 Jacinto, A., Martinez-Arias, A., and Martin, P. (2001). Mechanisms of epithelial
859 fusion and repair. *Nat Cell Biol* *3*, E117–E123.
- 860 Jay, P., Bergé-Lefranc, J.-L., Massacrier, A., Roessler, E., Wallis, D., Muenke, M.,
861 Gastaldi, M., Taviaux, S., Cau, P., and Berta, P. (2000). ARP3 β , the gene encoding
862 a new human actin-related protein, is alternatively spliced and predominantly
863 expressed in brain neuronal cells. *European Journal of Biochemistry* *267*, 2921–
864 2928.
- 865 Karin, M. (2009). NF- κ B as a Critical Link Between Inflammation and Cancer. *Cold*
866 *Spring Harb Perspect Biol* *1*.
- 867 Kurki, P., Vanderlaan, M., Dolbeare, F., Gray, J., and Tan, E.M. (1986). Expression
868 of proliferating cell nuclear antigen (PCNA)/cyclin during the cell cycle. *Exp. Cell*
869 *Res.* *166*, 209–219.

- 870 Lane, K., Valen, D.V., DeFelice, M.M., Macklin, D.N., Kudo, T., Jaimovich, A., Carr,
871 A., Meyer, T., Pe'er, D., Boutet, S.C., et al. (2017). Measuring Signaling and RNA-
872 Seq in the Same Cell Links Gene Expression to Dynamic Patterns of NF- κ B
873 Activation. *Cels* 4, 458-469.e5.
- 874 Ling, J., Kang, Y., Zhao, R., Xia, Q., Lee, D.-F., Chang, Z., Li, J., Peng, B.,
875 Fleming, J.B., Wang, H., et al. (2012). KrasG12D-Induced IKK2/ β /NF- κ B Activation
876 by IL-1 α and p62 Feedforward Loops Is Required for Development of Pancreatic
877 Ductal Adenocarcinoma. *Cancer Cell* 21, 105–120.
- 878 Melisi, D., Niu, J., Chang, Z., Xia, Q., Peng, B., Ishiyama, S., Evans, D.B., and
879 Chiao, P.J. (2009). Secreted interleukin-1alpha induces a metastatic phenotype in
880 pancreatic cancer by sustaining a constitutive activation of nuclear factor-kappaB.
881 *Mol. Cancer Res.* 7, 624–633.
- 882 Miralles, F., Posern, G., Zaromytidou, A.-I., and Treisman, R. (2003). Actin
883 Dynamics Control SRF Activity by Regulation of Its Coactivator MAL. *Cell* 113,
884 329–342.
- 885 Mullins, R.D., Heuser, J.A., and Pollard, T.D. (1998). The interaction of Arp2/3
886 complex with actin: Nucleation, high affinity pointed end capping, and formation of
887 branching networks of filaments. *PNAS* 95, 6181–6186.
- 888 Nelson, D.E., Ihekwebaba, A.E.C., Elliott, M., Johnson, J.R., Gibney, C.A., Foreman,
889 B.E., Nelson, G., See, V., Horton, C.A., Spiller, D.G., et al. (2004). Oscillations in
890 NF- κ B Signaling Control the Dynamics of Gene Expression. *Science* 306, 704–708.
- 891 Németh, Z.H., Deitch, E.A., Davidson, M.T., Szabó, C., Vizi, E.S., and Haskó, G.
892 (2004). Disruption of the actin cytoskeleton results in nuclear factor-kappaB
893 activation and inflammatory mediator production in cultured human intestinal
894 epithelial cells. *J. Cell. Physiol.* 200, 71–81.
- 895 Perona, R., Montaner, S., Saniger, L., Sánchez-Pérez, I., Bravo, R., and Lacal, J.C.
896 (1997). Activation of the nuclear factor-kappaB by Rho, CDC42, and Rac-1
897 proteins. *Genes Dev.* 11, 463–475.
- 898 Pires, B.R.B., Mencialha, A.L., Ferreira, G.M., de Souza, W.F., Morgado-Díaz, J.A.,
899 Maia, A.M., Corrêa, S., and Abdelhay, E.S.F.W. (2017). NF-kappaB Is Involved in
900 the Regulation of EMT Genes in Breast Cancer Cells. *PLoS One* 12, e0169622.
- 901 Pruyne, D., Evangelista, M., Yang, C., Bi, E., Zigmond, S., Bretscher, A., and
902 Boone, C. (2002). Role of formins in actin assembly: nucleation and barbed-end
903 association. *Science* 297, 612–615.
- 904 Rao, M.V., Chu, P.-H., Hahn, K.M., and Zaidel-Bar, R. (2013). An optogenetic tool
905 for the activation of endogenous diaphanous-related formins induces thickening of
906 stress fibers without an increase in contractility. *Cytoskeleton (Hoboken)* 70, 394–
907 407.
- 908 Rizvi, S.A., Neidt, E.M., Cui, J., Feiger, Z., Skau, C.T., Gardel, M.L., Kozmin, S.A.,
909 and Kovar, D.R. (2009). Identification and Characterization of a Small Molecule
910 Inhibitor of Formin-Mediated Actin Assembly. *Chemistry & Biology* 16, 1158–1168.

- 911 Rosette, C., and Karin, M. (1995). Cytoskeletal control of gene expression:
912 depolymerization of microtubules activates NF-kappa B. *J Cell Biol* 128, 1111–
913 1119.
- 914 Sachs, K., Perez, O., Pe'er, D., Lauffenburger, D.A., and Nolan, G.P. (2005).
915 Causal Protein-Signaling Networks Derived from Multiparameter Single-Cell Data.
916 *Science* 308, 523–529.
- 917 Sailem, H.Z., and Bakal, C. (2017). Identification of clinically predictive metagenes
918 that encode components of a network coupling cell shape to transcription by image-
919 omics. *Genome Res.* 27, 196–207.
- 920 Schliwa, M. (1982). Action of cytochalasin D on cytoskeletal networks. *Journal of*
921 *Cell Biology* 92, 79–91.
- 922 Scutari, M. (2010). Learning Bayesian Networks with the bnlearn R Package.
923 *Journal of Statistical Software* 35, 1–22.
- 924 Scutari, M., Graafland, C.E., and Gutierrez, J.M. (2018). Who Learns Better
925 Bayesian Network Structures: Constraint-Based, Score-based or Hybrid
926 Algorithms? *Proceedings of Machine Learning Research* 72, 416–427.
- 927 Sero, J.E., Sailem, H.Z., Ardy, R.C., Almuttaqi, H., Zhang, T., and Bakal, C. (2015).
928 Cell shape and the microenvironment regulate nuclear translocation of NF-κB in
929 breast epithelial and tumor cells. *Mol Syst Biol* 11.
- 930 Steele, C.W., Jamieson, N.B., Evans, T.R.J., McKay, C.J., Sansom, O.J., Morton,
931 J.P., and Carter, C.R. (2013). Exploiting inflammation for therapeutic gain in
932 pancreatic cancer. *Br J Cancer* 108, 997–1003.
- 933 Stehn, J.R., Haass, N.K., Bonello, T., Desouza, M., Kottyan, G., Treutlein, H.,
934 Zeng, J., Nascimento, P.R.B.B., Sequeira, V.B., Butler, T.L., et al. (2013). A Novel
935 Class of Anticancer Compounds Targets the Actin Cytoskeleton in Tumor Cells.
936 *Cancer Res* 73, 5169–5182.
- 937 Sun, S.C., Ganchi, P.A., Ballard, D.W., and Greene, W.C. (1993). NF-kappa B
938 controls expression of inhibitor I kappa B alpha: evidence for an inducible
939 autoregulatory pathway. *Science* 259, 1912–1915.
- 940 Tay, S., Hughey, J.J., Lee, T.K., Lipniacki, T., Quake, S.R., and Covert, M.W.
941 (2010). Single-cell NF-κB dynamics reveal digital activation and analog information
942 processing in cells. *Nature* 466, 267–271.
- 943 Thierry, J.P., and Sleeman, J.P. (2006). Complex networks orchestrate epithelial–
944 mesenchymal transitions. *Nat Rev Mol Cell Biol* 7, 131–142.
- 945 Tong, L., and Tergaonkar, V. (2014). Rho protein GTPases and their interactions
946 with NFκB: crossroads of inflammation and matrix biology. *Biosci Rep* 34, e00115.
- 947 Weichert, W., Boehm, M., Gekeler, V., Bahra, M., Langrehr, J., Neuhaus, P.,
948 Denkert, C., Imre, G., Weller, C., Hofmann, H.-P., et al. (2007). High expression of
949 RelA/p65 is associated with activation of nuclear factor-κB-dependent signaling in

950 pancreatic cancer and marks a patient population with poor prognosis. *British*
951 *Journal of Cancer* 97, 523–530.

952 Wickham, H. (2016). *ggplot2: Elegant Graphics for Data Analysis*.

953 Wu, C., Fernandez, S.A., Criswell, T., Chidiac, T.A., Guttridge, D., Villalona-Calero,
954 M., and Bekaii-Saab, T.S. (2013). Disrupting cytokine signaling in pancreatic
955 cancer: a phase I/II study of etanercept in combination with gemcitabine in patients
956 with advanced disease. *Pancreas* 42, 813–818.

957 Wu, P.-H., Gilkes, D.M., Phillip, J.M., Narkar, A., Cheng, T.W.-T., Marchand, J.,
958 Lee, M.-H., Li, R., and Wirtz, D. (2020). Single-cell morphology encodes metastatic
959 potential. *Science Advances* 6, eaaw6938.

960 Zambrano, S., De Toma, I., Piffer, A., Bianchi, M.E., and Agresti, A. (2016). NF- κ B
961 oscillations translate into functionally related patterns of gene expression. *ELife* 5.

962 Zandi, E., Rothwarf, D.M., Delhase, M., Hayakawa, M., and Karin, M. (1997). The
963 I κ B kinase complex (IKK) contains two kinase subunits, IKK α and
964 IKK β , necessary for I κ B phosphorylation and NF- κ B activation. *Cell*
965 91, 243–252.

966 Zhang, G., Gurtu, V., and Kain, S.R. (1996). An enhanced green fluorescent protein
967 allows sensitive detection of gene transfer in mammalian cells. *Biochem. Biophys.*
968 *Res. Commun.* 227, 707–711.

969 Zhao, X., Fan, W., Xu, Z., Chen, H., He, Y., Yang, G., Yang, G., Hu, H., Tang, S.,
970 Wang, P., et al. (2016). Inhibiting tumor necrosis factor- α diminishes
971 desmoplasia and inflammation to overcome chemoresistance in pancreatic ductal
972 adenocarcinoma. *Oncotarget* 7, 81110–81122.

973

Figure 1

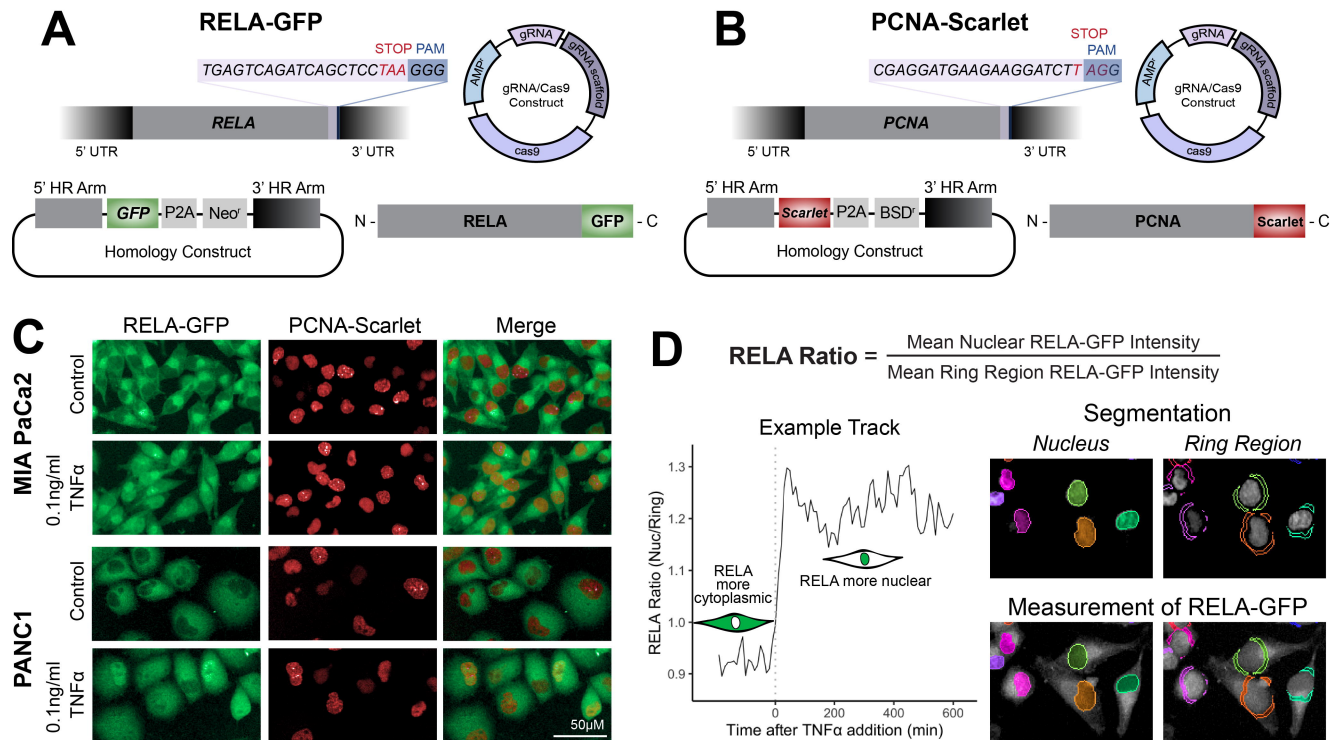


Figure 2

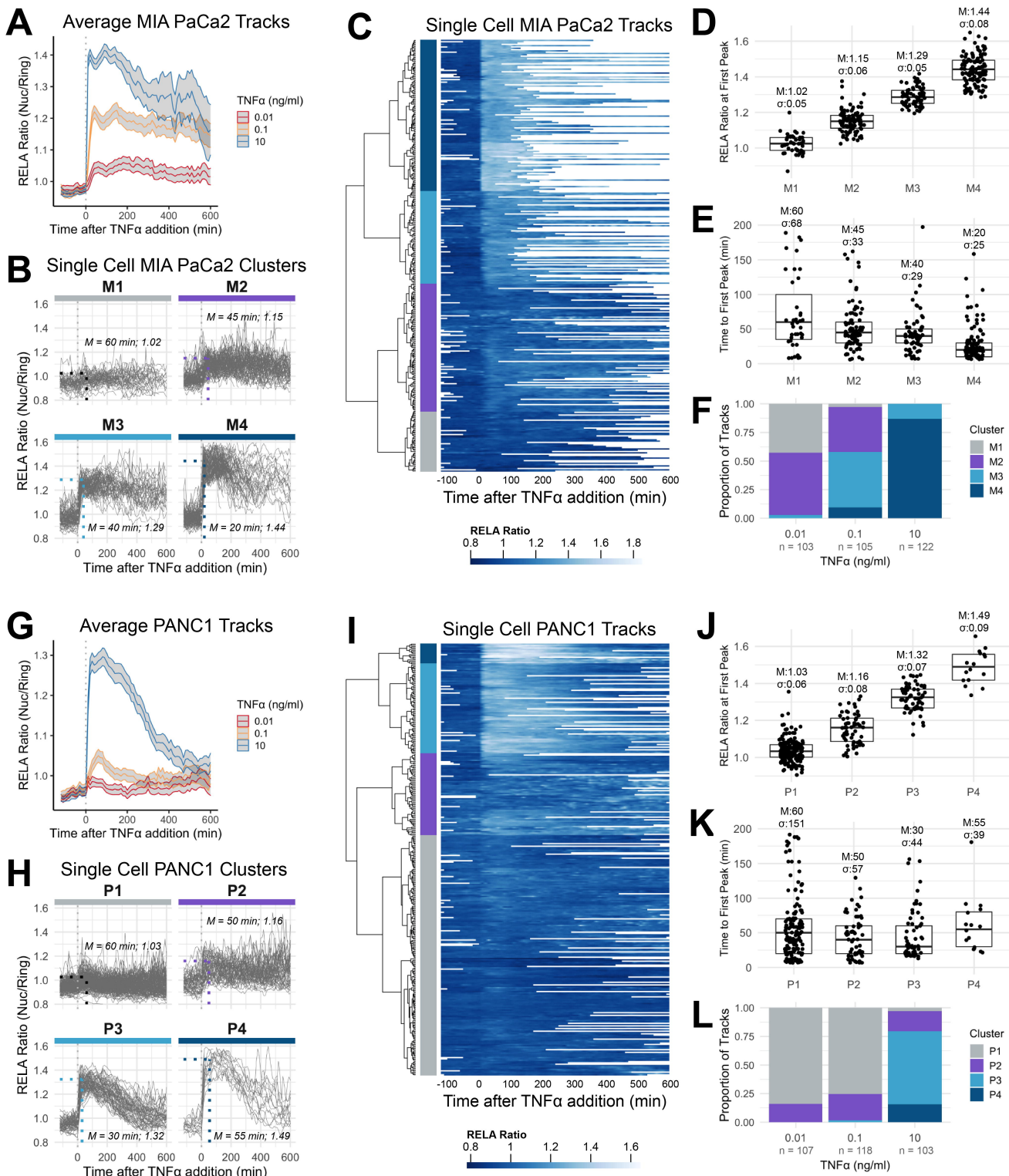
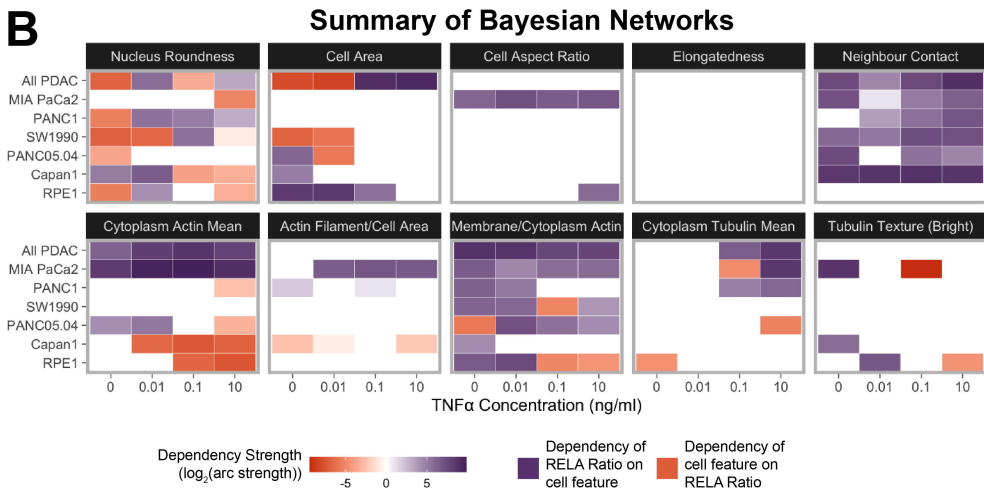
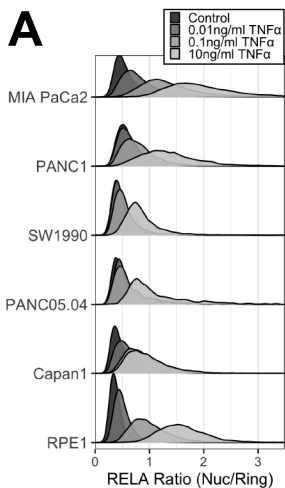


Figure 3



C Prediction of interline RELA ratio heterogeneity (All PDAC - 0.1ng/ml TNF α)

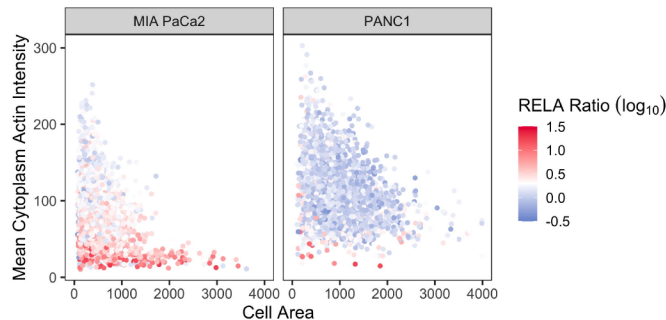
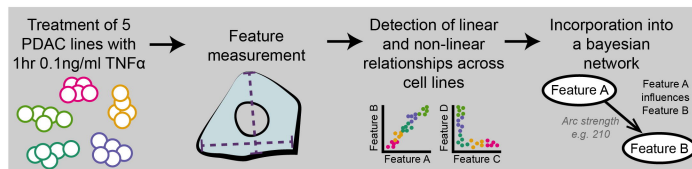
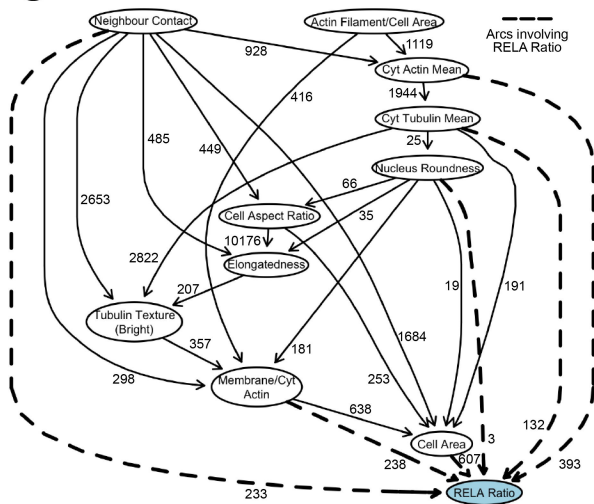
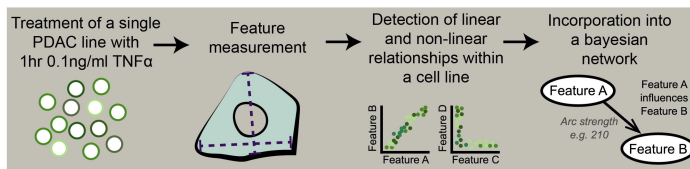


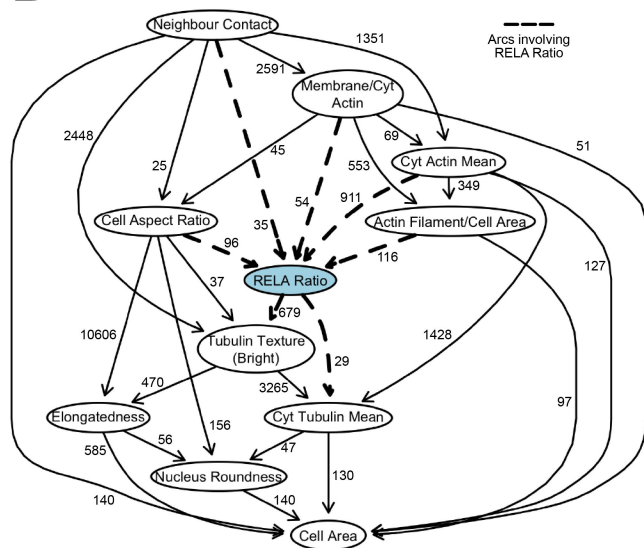
Figure 4

A Prediction of intraline RELA ratio heterogeneity (0.1ng/ml TNF α)



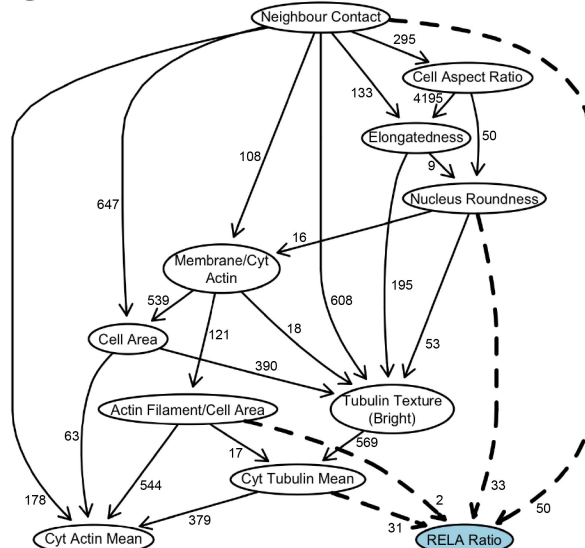
B

MIA PaCa2



C

PANC1



D

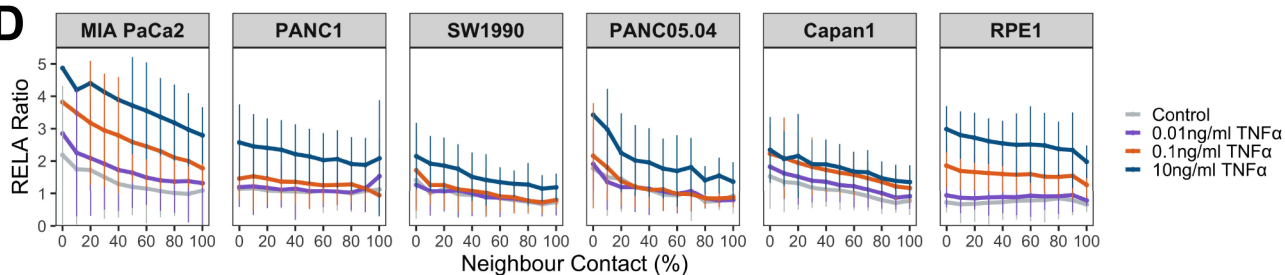


Figure 5

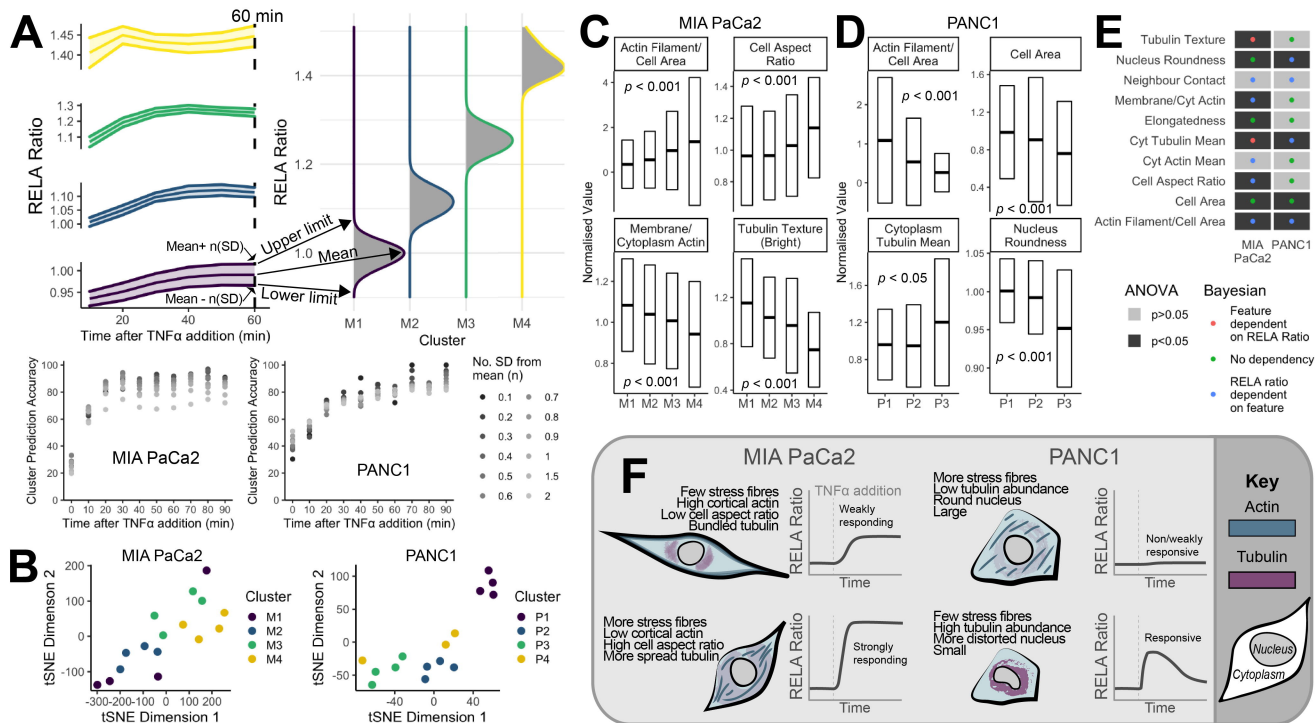


Figure 6

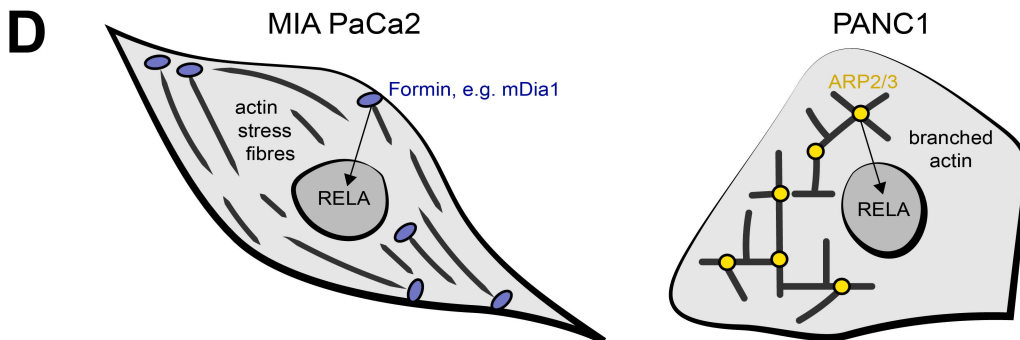
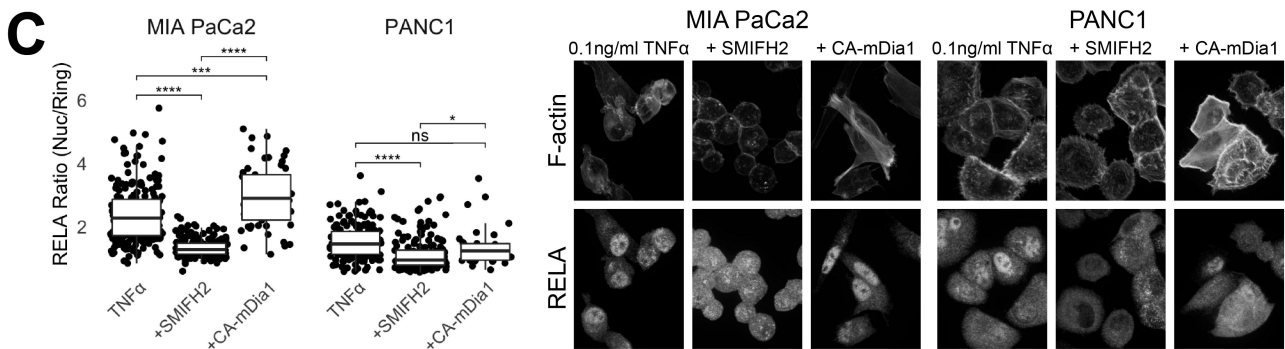
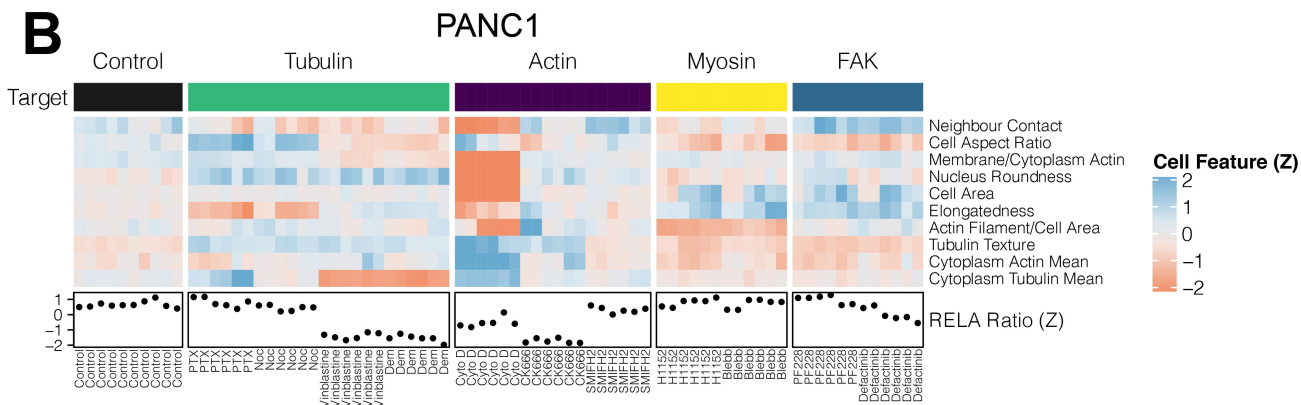
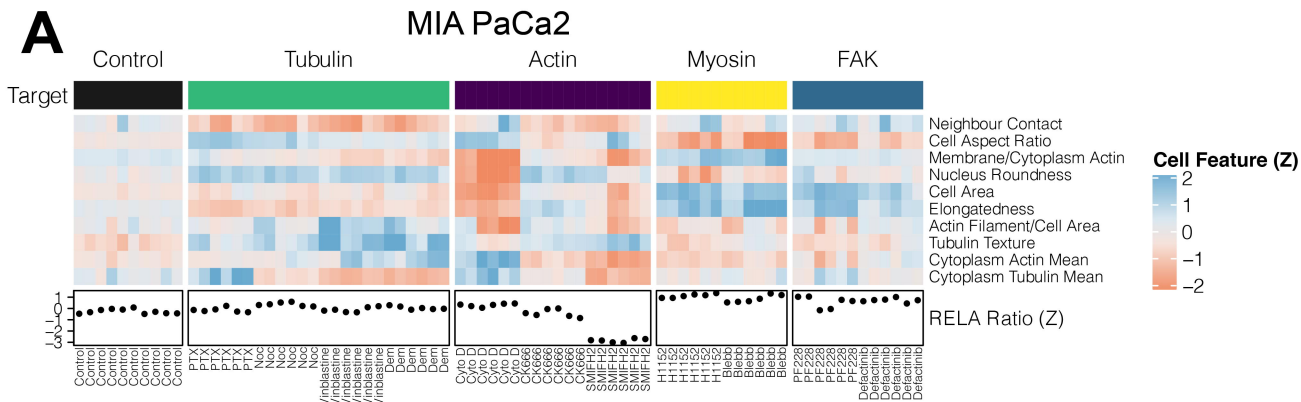


Figure S1

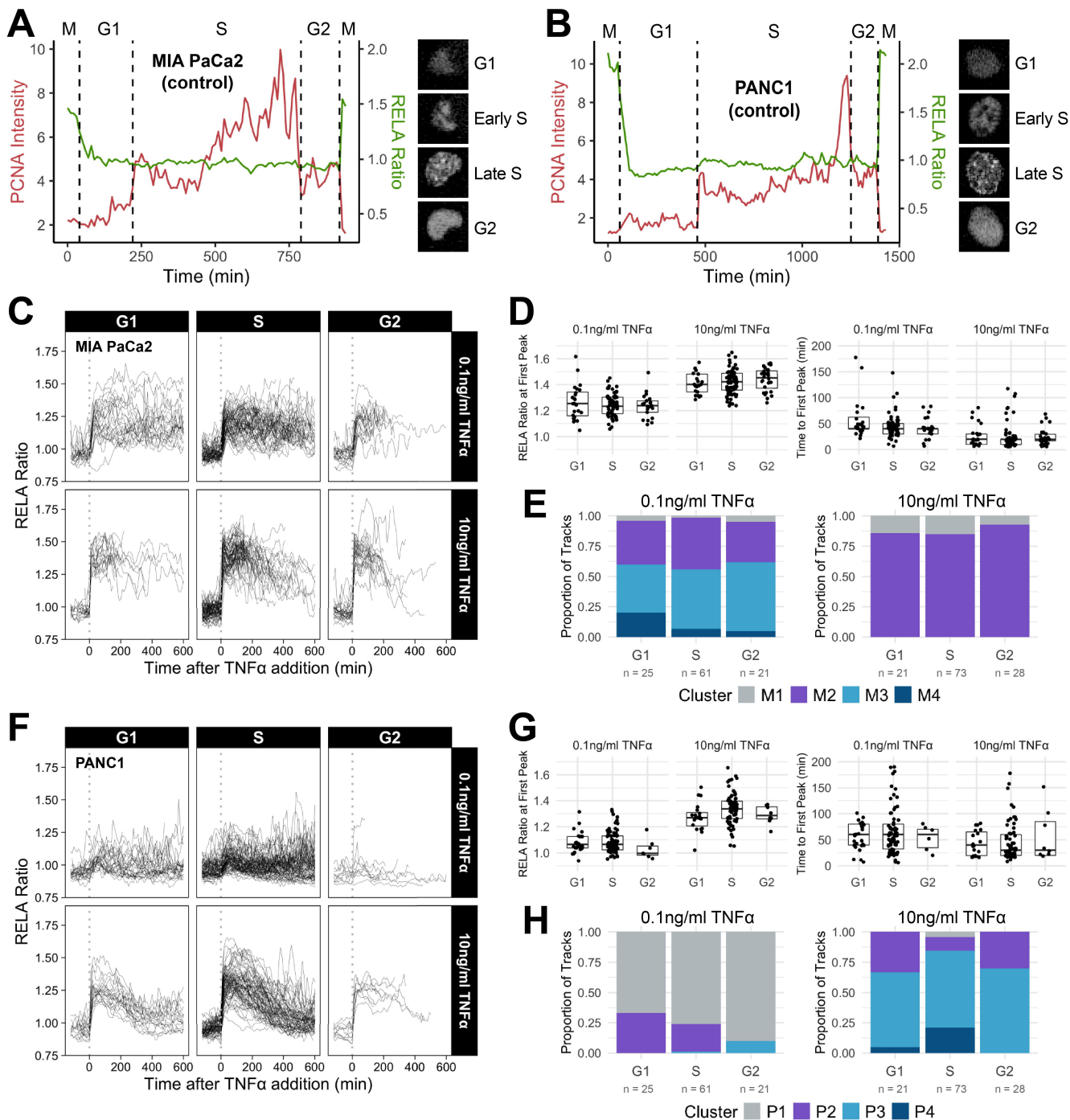
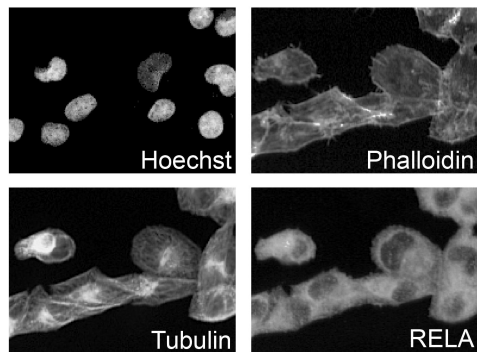
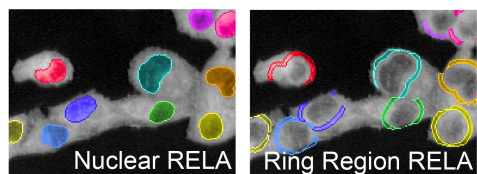


Figure S2

A Staining



B Automated image analysis of RELA localisation



$$\text{RELA Ratio} = \frac{\text{Mean Nuclear RELA Intensity}}{\text{Mean Ring Region RELA Intensity}}$$

C Independent Feature Selection

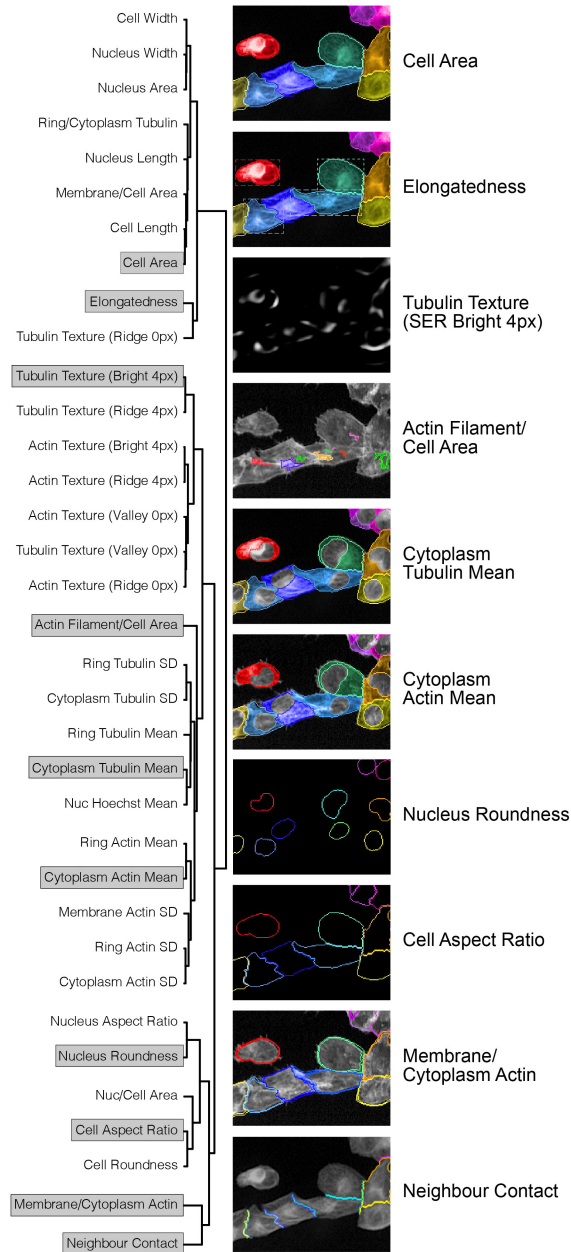
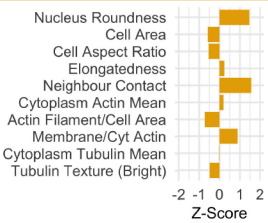
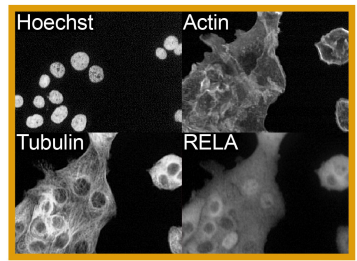
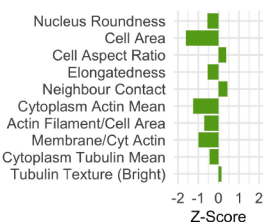
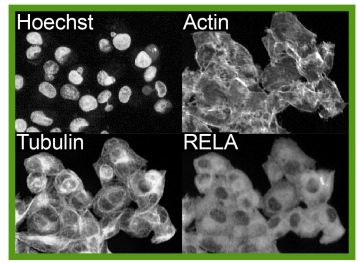


Figure S3

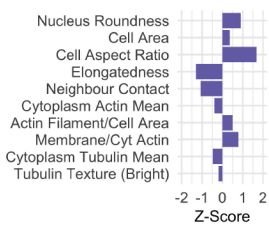
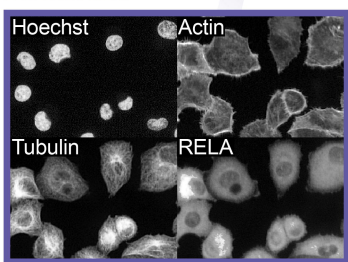
Capan1
 Form colonies
 Round nuclei
 Actin localised to cortex



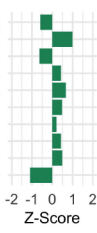
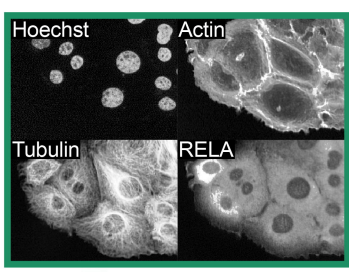
MIA PaCa2
 Small
 Low actin abundance
 Low attachment



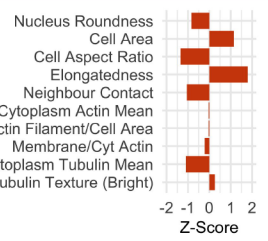
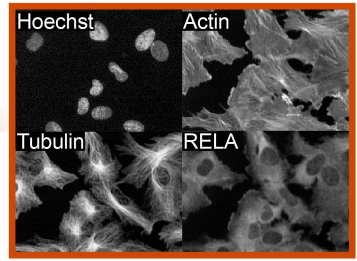
PANC1
 Flat
 Low cell-cell contact
 Single/unclustered
 Actin localised to membrane



SW1990
 Large
 Form colonies
 Low cell aspect ratio



RPE1
 Elongated
 Large
 Distorted nuclei
 Actin organised in stress fibres



PANC05.04
 High actin abundance
 Bundled tubulin

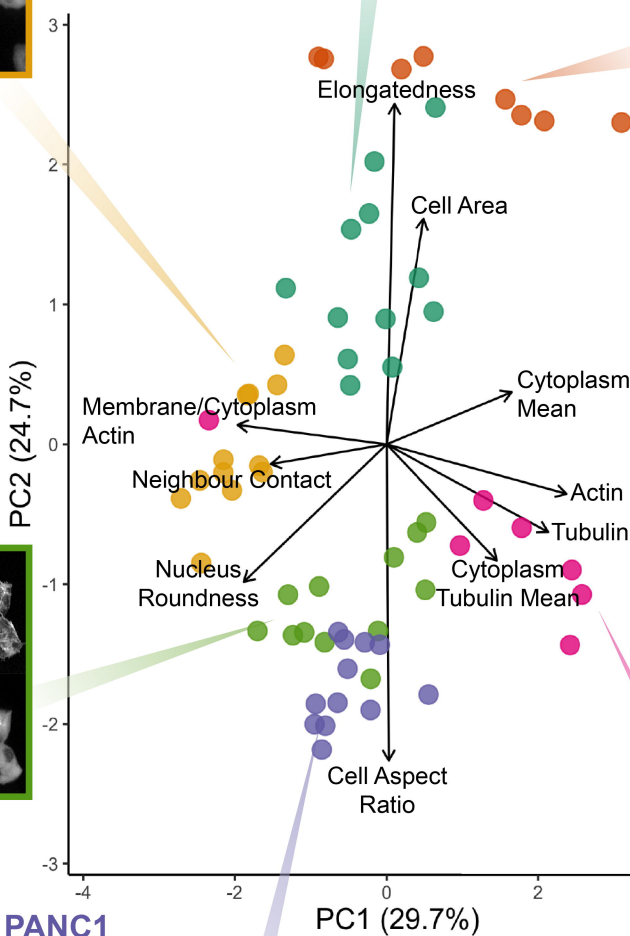
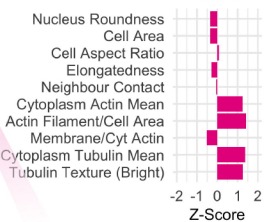
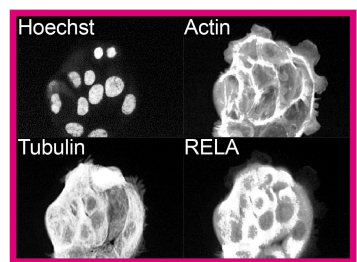


Figure S4

